Deep–Sea Research II 222 (2025) 105504

Contents lists available at ScienceDirect

Deep-Sea Research Part II

journal homepage: www.elsevier.com/locate/dsr2

Biogeochemical float deployment strategy in the Southwestern Indian ocean

Wilhem Riom [a,*], Vincent Taillandier [a], Céline Dimier [b], Fabrizio D'Ortenzio [a], Hervé Claustre [a]

[a] CNRS & Sorbonne Université, Laboratoire d'Océanographie de Villefranche (LOV), Villefranche-sur-Mer, France
[b] CNRS & Sorbonne Université, Institut de la Mer de Villefranche (IMEV), Villefranche-sur-Mer, France

ARTICLE INFO

Handling Editor: Prof. J Aristegui

Keywords:
BGC-Argo
Ocean observing systems
Southwestern Indian ocean

ABSTRACT

The recent roadmap *IndOOS-2* has stressed the need to expand the biogeochemical-Argo observing system in the Indian Ocean. The Monaco Explorations Indian Ocean expedition offered a unique opportunity to meet this goal in the southwestern sector which was, in this regard and at that time, one of the least covered oceanic regions. We designed a deployment strategy for the biogeochemical float array grounded on past experiences, existing knowledge, and the analysis of historical datasets to cover the contrasting biophysical regimes from the Seychelles Chagos Thermocline Ridge to the subtropical gyre. Aligning with IndOOS-2 recommendations, a denser float distribution was set in the tropical band to enhance biogeochemical observations in upwelling zones. Following this strategy, a fleet of seventeen biogeochemical floats was successfully deployed during the expedition in October–November 2022. After two years of operations, the spatio-temporal distribution covered by the fleet confirmed that the goals of the deployment strategy have been reached, revealing seasonal modulations of the meridional trophic gradient with respect to phytoplankton biomass from tropical mesotrophy to subtropical oligotrophy.

1. Introduction

Observing the oceans is one of the most challenging issues in present-day Earth sciences. Although satellites significantly mitigate the chronic lack of ocean data (Munk, 2000; McClain, 2009; Groom et al., 2019; Shutler et al., 2024), space-based observations, confined to the sea surface, leave much of the ocean's interior largely unexplored (Martin et al., 2020).

The Argo program represented an impressive step forward in filling these gaps by implementing a systematic observation network able to monitor temperature and salinity within the upper 2 km of the global ocean (Roemmich et al., 2009, 2019; Wong et al., 2020). Its biogeochemical component, BGC-Argo, operates profiling floats equipped with biogeochemical sensors (Claustre et al., 2020; Chai et al., 2020). The BGC-Argo program is currently in a global implementation phase (Biogeochemical-Argo Planning Group, 2016), following nearly a decade of technological developments and regional pilot studies, such as NAOS in the Mediterranean Sea (D'Ortenzio et al., 2020) or SOCCOM in the Southern Ocean (Sarmiento et al., 2023).

Despite advancements achieved by remote sensing and in-situ automated systems (Le Traon, 2013; Riser et al., 2016; Johnson et al., 2022), ship-based observations remain essential to develop reference data collections. In this respect, international research programs are crucial to sustain these *in-situ* observational efforts. Such initiatives have coordinated repeated oceanographic sections like the Global Ocean Ship-Based Hydrographic Investigation Program (GO-SHIP, Talley et al., 2017; Sloyan et al., 2019), building on the success of the World Ocean Circulation Experiment (WOCE, Thompson et al., 2001) and Climate and Ocean: Variability, Predictability, and Change project (CLIVAR). They have also supported the implementation of time series as part of long-term observatories, such as Ocean Weather Station Papa (Freeland, 2007), the Hawaii Ocean Time-series program (HOT, Karl and Roger, 1996), and DYFAMED (Coppola et al., 2024).

Overall, international and regional efforts provided the framework to identify, set up and implement observing systems. Nowadays, with the support of UNESCO, these actions are progressively integrated

This article is part of a special issue entitled: ME-IO published in Deep-Sea Research Part II.

* Corresponding author.
E-mail address: wilhem.riom@imev-mer.fr (W. Riom).

https://doi.org/10.1016/j.dsr2.2025.105504
Received 31 October 2024; Received in revised form 6 June 2025; Accepted 21 June 2025
Available online 24 June 2025

worldwide as the Global Ocean Observing System (GOOS, Dexter and Summerhayes, 2010; Moltmann et al., 2019; Tanhua et al., 2019). The GOOS successful implementation relies on regional initiatives and on the capacity to account for scientific and technological specificities. In this regard, the Indian Ocean Observing System (IndOOS) is one of the main regional components of this global organizational structure. It has coordinated observational efforts over the Indian Ocean during the first decade of the 21st century, through several international hydrographic surveys (McPhaden et al., 2024).

The IndOOS-2 consortium recently reviewed successes and failures of the initial design (IndOOS-2 Full Report, 2019, Beal et al., 2020; Hermes et al., 2019). Among them, the severe lack of biogeochemical observations in the Indian Ocean was highlighted, especially in the southern hemisphere, leaving ocean-colour satellite as the only regular and continuous source of biogeochemical data (Lévy et al., 2007; Resplandy et al., 2009; George et al., 2018; Guo et al., 2022). In response, the consortium proposed a roadmap for the horizon 2030 in order to address the needs for expansion of IndOOS components. This is particularly the case of the Argo network which is relatively coarse compared to other oceanic basins. In its actionable recommendation A1 of tier II (Extend IndOOS capacities to better address scientific and operational drivers, (IndOOS-2 Full Report, 2019)), the consortium dimensioned 200 active BGC-Argo floats throughout the Indian Ocean, with priority deployments in productive regions such as upwellings (Vinayachandran et al., 2021).

In a close perspective, the roadmap intends to anticipate societal needs for adaptation and resilience to climate change. This is particularly relevant in the Southwestern Indian Ocean (SWIO), where food resources mainly depend on fisheries (Moustahfid et al., 2018; Taylor et al., 2019) which are conditioned by primary production (Pauly and Christensen, 1995; Chassot et al., 2010; Marshak and Link, 2021; Marsac et al., 2024). Therefore, given the major climatic signals affecting this region (Saji et al., 1999; Roxy et al., 2014; Vidya et al., 2020; Dalpadado et al., 2024), enhanced monitoring of marine ecosystems becomes essential.

In this context, the Indian Ocean expedition conducted by Monaco Explorations in October–November 2022 (hereinafter the ME-IO cruise) supported the deployment of seventeen BGC-Argo floats over the SWIO. This study relates the preparation and the outcomes of this initiative. Section 3 outlines the design of the array: the deployment strategy tailored for the ME-IO cruise, based on previous experiences (Talley et al., 2019; D'Ortenzio et al., 2020) that intends to meet the actionable recommendations of the IndOOS-2 roadmap. In Section 4, the spring-time hydrography of the SWIO is described using the dataset collected during the ME-IO cruise. The seasonal modulations of its biogeochemical conditions are drawn using the BGC-Argo array dataset after two years of operations. Finally, the deployment strategy is discussed in Section 5, offering guidelines for future deployments in the SWIO.

2. Material and methods

The study region, referred hereinafter to as the SWIO, extends meridionally between the Equator and 40°S, and zonally between 30°E and 80°E (Fig. 1a). The datasets presented hereafter were extracted exclusively within these geographical boundaries. The Mozambique Channel and the Mozambique Basin were excluded from the study region. The bioregionalization used for the deployment strategy is presented in Section 2.1. The data collections of the ME-IO cruise are described in Section 2.2. Argo and BGC-Argo data collections are presented in Section 2.3. The diagnostic tools used in the analysis are detailed in Section 2.4.

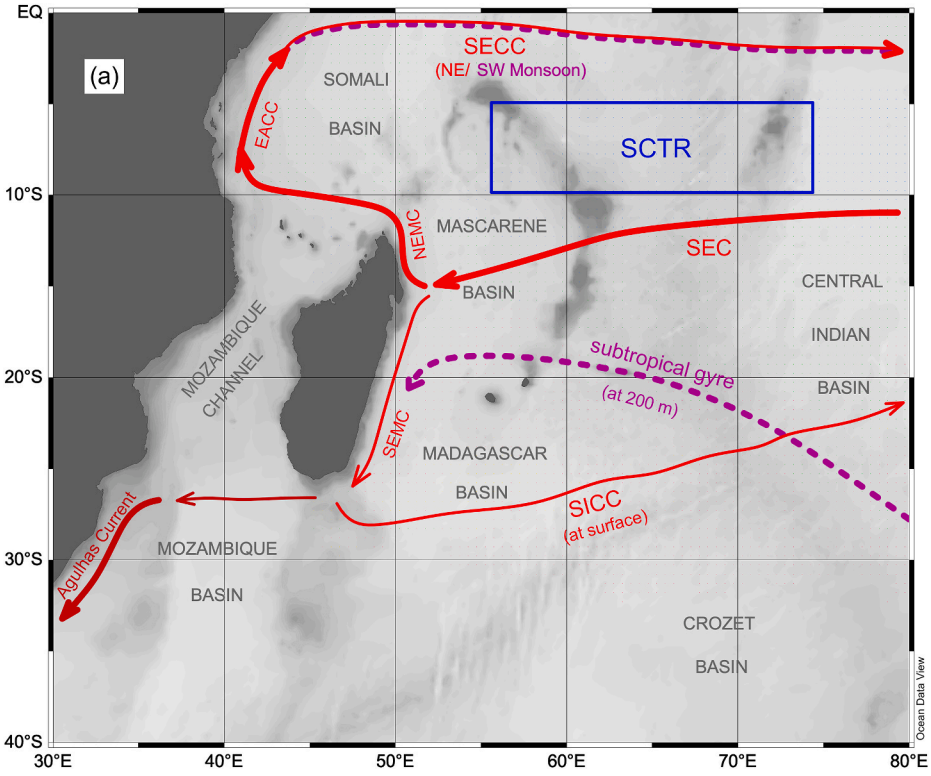

Fig. 1. a) schematic diagram assembling the main currents and oceanographic features over the SWIO. b) mean dynamic topography at 10 dbar relative to 1000 dbar (in dyn·m). c) mean dynamic topography at 400 dbar relative to 1000 dbar (in dyn·m). d) meridional section of temperature (°C), isopycnals 24.8, 26.0, 26.8 indicated in black lines, section location indicated by the red box in inset. e) same as (d) for salinity; Subtropical Underwater (STUW), Central Water (CW), Antarctic intermediate water (AAIW) and Red Sea overflow water (RSOW) are indicated. f) same as (d) for oxygen concentration (μmol·kg^{-1}). g) same as (d) for nitrate concentrations (μmol·kg^{-1}). (For interpretation of the references to colour in this figure legend, the reader is referred to the Web version of this article.)

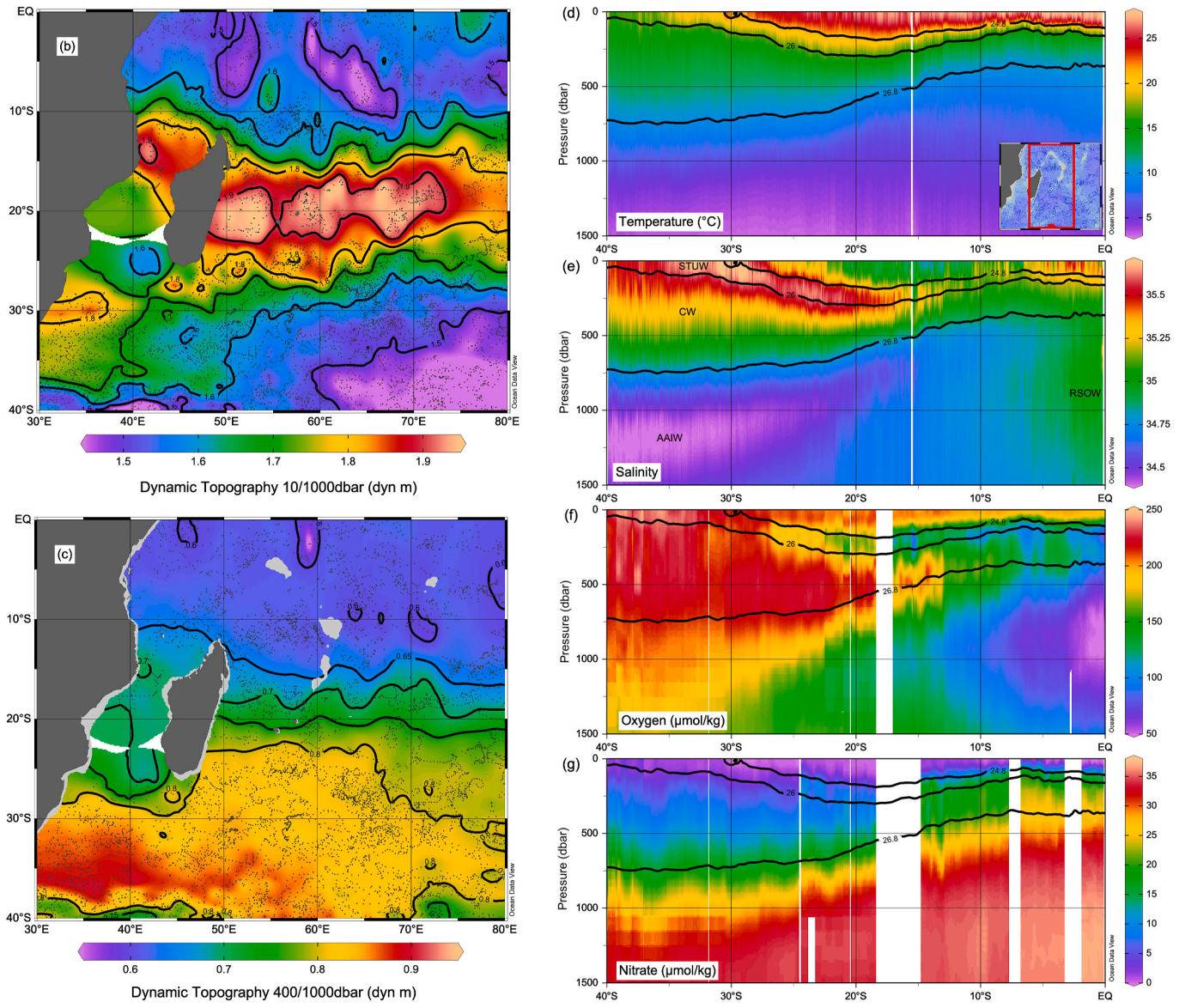

Fig. 1. (*continued*).

2.1. Bioregionalization of the SWIO using satellite ocean colour

A climatology was set up over the SWIO following the procedure described in Baudena et al. (2025) using surface chlorophyll concentrations from ocean colour satellites (ChlSat) as provided in the CMEMS catalogue (Globcolour L3 product). Annual cycles of ChlSat were derived at a weekly resolution by averaging available data over the period October 2022–September 2024 and within pixels of resolution 0.5°. Normalized annual ChlSat cycles were computed by dividing each time series by its annual maximum.

The Ocean colour climatology was partitioned into four clusters using the k-means algorithm (Hartigan and Wong, 1979; Ahmed et al., 2020) following the methodology successfully applied in D'Ortenzio and Ribera d'Alcalà (2009), Marchese et al. (2019), Mayot et al. (2016), Kheireddine et al. (2021), Ardyna et al. (2017), D'Ortenzio et al. (2012), and Baudena et al. (2025). These clusters form subgroups, assembled together according to similar seasonal patterns. As detailed in the Supplementary Material C, a partition into four clusters was found to be optimal, and led to distinct seasonal patterns (Figure C2b) associated with spatial extensions covering the SWIO (Figure C2a).

2.2. Ship-borne reference datasets

The ME-IO expedition was conducted on board the S.A. Agulhas II and supported a multi-disciplinary panel of field activities. Among them, oceanographic stations were carried out down to 2000 m depth using a CTD-rosette composed of a carousel of 24 Niskin bottles, and a Sea-Bird SBE911+ underwater unit. High accuracy sensors allowed measurement of pressure, temperature, conductivity, oxygen, nitrate, beam transmission and chlorophyll fluorescence at 24 Hz resolution. Sensors' data were processed into 1-m resolution vertical profiles as in Taillandier et al. (2018). Salinity and potential density anomaly referenced to the surface (hereafter designated as density) were derived from the primary CTD measurements. Water samples collected by the Niskin bottles were taken for quantification of biogenic elements (dissolved oxygen, macronutrients, salinity, alkalinity and pH) and pigment concentrations at discrete depth levels. CTD profiles and laboratory measurements were processed post-cruise and freely distributed into quality-controlled scientific data collections (Taillandier et al., 2024).

For phytoplankton pigment determination, seawater samples of 2.7 L were filtered through Whatman GF/F filters (0.7 µm pore size). Filters were immediately flash-frozen in liquid nitrogen before storage at

−80 °C, then transported in liquid nitrogen dry shippers to the SAPIGH national high performance liquid chromatography (HPLC) analytical service at the *Institut de la Mer de Villefranche*. Pigment extraction and analysis were carried out according to the method described in Ras et al. (2008). Total chlorophyll-a (TChl-a) sums chlorophyll-a (Chl-a) and divinyl-Chlorophyll-a (DVChl-a). TChl-a is the universal proxy for phytoplankton biomass and supports the *in-situ* calibration of the fluorometers that equip the CTD-rosette and the BGC-Argo floats (Supplementary Material A). Accessory pigments (other chlorophylls and carotenoids) are specific to phytoplankton groups and their respective proportions to TChl-a serve as a proxy of the community composition. Eight pigments were used as biomarkers of several phytoplankton taxa: DVChl-a (prochlorophytes), peridinin (dinoflagellates), fucoxanthin (diatoms), alloxanthin (cryptophytes), zeaxanthin (cyanobacteria, prochlorophytes), 19′-butanoyloxyfucoxanthin (19′-But, pelagophytes, prymnesiophytes), 19′-hexanoyloxyfucoxanthin (19′-Hex, prymnesiophytes) and Chl-b (chlorophytes).

2.3. Argo and BGC-Argo data collections

The Argo program sustains a global array of physical and biogeochemical autonomous sensors over a fleet of freely drifting profiling floats (Owens et al., 2022). The BGC-Argo floats measure pressure, salinity and temperature over the first 2 km of the water column, together with essential biogeochemical variables: pH, oxygen, nitrate, chlorophyll fluorescence, particle backscattering, and downwelling irradiance (Bittig et al., 2019). Collected datasets are quality-controlled and freely distributed by the different data assembly centers of the Argo program (Argo, 2000).

To support the results presented in Section 3.1, all the Argo profiles collected within the SWIO region (extending from the Equator and 40°S and from 30°E to 80°E) between October 2022 and September 2024 were considered to provide contemporary distributions of temperature, salinity, oxygen, and nitrate concentrations in the upper 1.5 km layer (302 floats and 8518 profiles). When available, Argo data in adjusted delayed mode were prioritized over real-time data.

Seventeen BGC-Argo floats were deployed at reference oceanographic stations occupied during the ME-IO expedition (Table 1). Metrological verification and interoperability of the autonomous fluorescence sensors were performed versus the HPLC dataset and a scale factor was estimated for each individual sensor (Supplementary Material A). After two years of operation, thirteen floats stayed in their deployment zone for more than a year while four floats left their deployment zone. Only the first group has been considered for the subsequent analysis of phytoplankton cycles presented in Section 4.3. This selection provides twenty-four annual cycles individually collected and referenced to the ship-borne measurements.

2.4. Diagnostics

Applied to the Argo data selection, dynamic height (in dyn·m) relative to a reference geopotential at 1000 dbar was computed as the integral of specific volume anomalies between 10 and 1000 dbar and between 400 and 1000 dbar. Horizontal mapping of this quantity indicates circulations tangential to the contours; gradients normal to contours allow the sizing of geostrophic currents at surface, and at 400 m depth (Pond and Pickard, 1983). Interpolation of dynamic topography was performed using a weighted average gridding method (provided by

Table 1
List of the 17 BGC-Argo floats deployed during the ME-IO expedition. Sensors: optode for oxygen (O), ECO-triplet for Chl-a fluorescence (A); SUNA for nitrate (N). Regional distribution: Seychelles Chagos Thermocline Ridge (SCTR), South Equatorial Current (SEC), subtropical gyre (STG), Madagascar Bloom (MB).

FLEET STATUS							DEPLOYMENT			
WMO	Project	Sensors	Number of profiles	Period	Resolution (in days)	Regional distribution	Date	Latitude	Longitude	Scale factor TChla-FChla
3902471	REFINE	OA	45	01/11/22–27/11/23	8.7	SCTR 344 profiles (39 %) 9 annual cycles	2022-11-02	5°59.910′S	59°59.524′E	0.9
5906539	GO-BGC	NOA	70	02/11/22-21/09/24	9.9		2022-11-02	5°59.831′S	59°59.606′E	0.7
6990504	MONACO	OA	70	01/11/22–24/09/24	9.9		2022-11-02	5°59.515′S	60°00.379′E	0.85
4902623	CANADA	OA	69	28/10/22-08/09/24	9.9		2022-10-28	5°30.041′S	52°00.093′E	1.35
6990503	REFINE	OA	90	28/10/22–25/09/24	7.8		2022-10-28	5°30.114′S	52°00.164′E	1
4902626	CANADA	OA	70	18/10/22-08/09/24	9.9	SEC 354 profiles (41 %) 10 annual cycles	2022-10-18	10°45.057′S	50°00.246′E	0.7
5906537	GO-BGC	NOA	68	18/11/22-17/09/24	9.9		2022-11-17	12°28.000′S	60°32.379′E	0.7
5906540	GO-BGC	NOA	71	27/10/22–25/09/24	9.9		2022-10-27	8°00.000′S	48°30.000′E	0.7
5906970	REFINE	NOA	73	16/10/22-22/09/24	9.7		2022-10-16	12°40.220′S	53°30.021′E	0.7
6990505	NAOS	NOA	72	16/10/22-17/09/24	9.8		2022-10-16	12°40.126′S	53°29.927′E	0.85
4902620	CANADA	OA	70	16/10/22-05/09/24	9.9	STG 107 profiles (12 %) 3 annual cycles	2022-10-15	19°30.102′S	54°59.991′E	1.15
5906536	GO-BGC	NOA	37	15/10/22-21/10/23	10.1		2022-10-15	19°30.102′S	54°59.991′E	1.45
5906538	GO-BGC	NOA	68	27/11/22–24/09/24	9.8	MB 68 profiles (8 %) 2 annual cycles	2022-11-26	27°20.029′S	49°59.938′E	1.15
5906971	NAOS	NOA	70	28/11/22-05/09/24	9.2	STG 0 annual cycle	2022-11-27	32°00.126′S	39°59.729′E	–
3902472	MONACO	OA	67	26/11/22-05/09/24	9.7	MB 0 annual cycle	2022-11-25	24°59.573′S	53°00.547′E	–
4902628	CANADA	OA	66	22/11/22-05/09/24	9.9	SEC 0 annual cycle	2022-11-21	18°14.998′S	58°30.026′E	–
5906972	NAOS	NOA	76	22/10/22-05/09/24	8.6	SEC 0 annual cycle	2022-10-21	10°18.401′S	44°47.753′E	–

the software *Ocean Data View v5.7*) with an isotropic correlation length 1.75°. No specific extrapolation was applied toward the coasts, only subsequent masking of land pixels.

Meridional sections of temperature, salinity, oxygen, and nitrate were plotted considering a subset of profiles extracted inside the zonal extension of the Mascarene Basin. Field interpolation from the surface down to 1500 m depth was performed using a weighted average gridding method (provided by the software *Ocean Data View v5.7*) with a horizontal correlation length 0.4° and a vertical correlation length of 20 m.

The mixed layer depth (MLD) was estimated from the density profiles as the depth where the residual mass content (i.e., the vertical integral of the density anomaly relative to surface) was equal to 1 kg m^{-2} (Prieur et al., 2020). This buoyancy criterion was preferred to alternative approaches such as a threshold density deviation to surface density of 0.03 kg m^{-3} (e.g., D'Ortenzio et al., 2005), in order to filter out short-term temporal variability of the mixed layer (notably its diurnal cycle) and reduce sensitivity to transient pycnoclines. The depth of three isopycnals of interest was retrieved from every density profile measured by the CTD-Rosette and the Argo floats. Deep chlorophyll maximum (DCM), surface Chl-a, and vertically integrated Chl-a in the first 400 m of the water column were computed from calibrated Chl-a fluorescence profiles, following Mignot et al. (2014).

Diagnostics of residence times and connectivity were computed using all the Argo floats crossing the SWIO during more than a month. Overall, 1376 trajectories were extracted from the historical Argo data collection. The mean residence times were calculated as the average time spent by floats within each bioregion. Fates of individual trajectories were assembled to give a statistical view of the connectivity between bioregions. Results of the Lagrangian analysis are detailed in the Supplementary Material D.

3. Deployment strategy

This section reports the setup of the deployment strategy with respect to: i) physical and biogeochemical contrasts over the SWIO reviewed from current knowledge and historical datasets; ii) specifics of the ME-IO cruise planning and the number of floats provided by the BGC-Argo program.

3.1. Review of circulation and water masses

Current knowledge depicts the SWIO as a major crossroad of the global ocean thermohaline circulation, where large-scale current systems over the equatorial band, the subtropical gyre, and the circumpolar circulation interplay (Talley et al., 2011; Hernández-Guerra and Talley, 2016; Phillips et al., 2024). In addition, the presence of numerous islands, banks, ridges and seamounts divide up the regional topography in three deep sub-basins interconnected by steep trenches or shallow sills (Fig. 1a): i) the Mozambique Basin, southern extension of the Mozambique Channel between Madagascar and the eastern African coast; ii) the Mascarene Basin located between the Mascarene Arc (Seychelles islands, Saya de Malha bank, Mauritius islands, La Réunion) and Madagascar; iii) the Madagascar Basin located southeast of the eponymous island and bounded to the south by the Southwest Indian Ridge.

Because of such a complex hydrodynamic environment, the characterization of oceanographic features can differ between reports, notably in terms of presence, location or persistence (Stramma and Lutjeharms, 1997; Schott et al., 2002; Reid, 2003; Schott et al., 2009; Talley et al., 2011; Phillips et al., 2021; Hood et al., 2024). Little is known about seasonal variability apart from the influence of the monsoon (Schott and Julian, 2001; Tripathy et al., 2020). Hence, a schematic climatological circulation diagram, supported by and in agreement with the analysis of the historical Argo dataset, is drawn in Fig. 1a. It is composed of three regional-scale circulation cells that occupy the meridional extension of the SWIO between the Equator and 40°S.

At low latitudes, a cyclonic cell spreads over the tropical band, as shown by low dynamic height at surface and at 400 m depth (Fig. 1b and c). Associated with the tightening of isolines (Fig. 1b), the South Equatorial Current (SEC) flows westward at about 12°S across the Central Indian Basin, carrying nutrient-rich and cool surface waters from the Indonesian Through Flow (New et al., 2005). The SEC bends southwestward across the Mascarene Arc (Coopen et al., 2022), then reaches Madagascar at about 15°S where it splits in two branches (Yamagami and Tozuka, 2015). The northward branch, so-called North East Madagascar Current (NEMC), flows into the Somali Basin where it connects with the East African Coastal Current (EACC). In continuity along the Equator, the South Equatorial Counter Current (SECC) flows eastward at the surface during the Northeast Monsoon, and in subsurface during the Southwest Monsoon (Hermes and Reason, 2008; Yokoi et al., 2008; Schott et al., 2009). In the inner part of the cyclonic cell known as the Seychelles Chagos Thermocline Ridge (SCTR, Aguiar-González et al., 2016), the thermocline shallows which infers nutrient-rich and productive conditions into the sunlit layer.

At higher latitudes, the anticyclonic subtropical gyre is shown by high dynamic height at 400 m depth (Fig. 1c). The gyre extends over the whole Mozambique Basin, delineated by the Agulhas Current and its retroflexion along the 40°S parallel. It also occupies the Madagascar Basin and the southern part of the Mascarene Basin, delineated at 400 m depth by a westward flow along 20°S connecting with the South East Madagascar Current (SEMC). SEMC reaches downstream the Agulhas Current at the southern opening of the Mozambique Channel (Vianello et al., 2020). On top of this feature, the surface dynamic topography (Fig. 1b) indicates low values over the Crozet Basin and high values north of the South Indian Counter Current (SICC, Menezes et al., 2014) that flows northeastward from the southern tip of Madagascar.

This third anticyclonic cell, so-called hereinafter *Mascarene bowl*, is a regional-scale feature of the surface circulation, with limited depth extent in absence of signature at 400 m depth (Fig. 1b), located in a latitudinal band between the SCTR and the subtropical gyre. Interestingly, the Mascarene bowl is spatially disconnected with the SCTR, but not with the subtropical gyre. It lays over the subtropical gyre in the Mascarene Basin and part of the Madagascar Basin, possibly as a regional response of the large-scale circulation systems to the presence of Madagascar (Nagura and McPhaden, 2018).

The three circulation cells would shape the distribution of seawater properties in the upper oceanic layer (Talley and Baringer, 1997). Meridional sections of temperature, salinity, oxygen and nitrate concentrations are respectively drawn in Fig. 1d,e,f,g by aggregating every Argo data inside the Madagascar and Mascarene Basins. The Central Water (CW) composes the permanent thermocline by Subtropical Underwater (STUW) associated to a salinity maximum and by slightly denser Subtropical Mode Water (STMW) corresponding to a water body of homogeneous density 26.0. Below the thermocline, Antarctic Intermediate Water (AAIW) associated to a salinity minimum and Red Sea Overflow Water (RSOW) characterized by a local salinity maximum and oxygen minimum can be identified respectively at high and low latitudes of the section.

Along the meridional transect, CW remains delineated by isopycnals 24.8 and 26.8. At the upper vertical bound, isopycnal 24.8 interfaces CW with surface waters, which are nitrate-depleted and oxygenated. Just below this interface, STUW (formed in the subtropical gyre, Talley et al., 2011) and STMW (formed slightly more south at the subtropical front, Schott and McCreary, 2001) are poor in preformed nitrate. The two water masses get progressively enriched and deoxygenated by remineralization as they subduct north of 30°S. At the lower vertical bound, isopycnal 26.8 interfaces CW with denser water bodies at intermediate depth. AAIW (formed at 1000 m depth in the confluence of the southwest Atlantic at the polar front, Fine, 1993; Nagura and McPhaden, 2018) progressively shallows northwards in the section up to 600 m depth. North of 15°S, its properties are progressively altered by mixing

with RSOW: salinity increases below the thermocline, with less oxygenated conditions and slightly higher nitrate concentrations.

The shape of the permanent thermocline can be characterized by three isopycnals 24.8, 26.8 associated to vertical extension of CW, and 26.0 associated to STMW. At high latitudes, the thermocline is 700 m thick and gradual; gets sharper (300 m thick) and steeper at low latitudes. This latitudinal change is in agreement with the presence and the extension of the anticyclonic subtropical gyre. Moreover, the upper thermocline deepens down to 200 m depth at 30°S; it is found shallow, into the first 10 m, north of 15°S. This pattern is in agreement with the presence and extensions of the anticyclonic Mascarene bowl and the cyclonic SCTR.

3.2. Provisional plan of deployment

The ME-IO expedition was designed as a multidisciplinary research cruise lasting two months (October 1st – November 30th, 2022), with departure and arrival at Cape Town (South Africa). Four port calls were planned in SWIO islands with respect to other scientific activities: La Réunion (France), Aldabra, Mahé (Seychelles), and Mauritius.

In 2022, the SWIO one of the oceanic region the least covered by the BGC-Argo array. Hence, with the opportunity to survey the whole sector onboard the large research vessel S.A. Agulhas II, a total of 17 profiling floats equipped with biogeochemical sensors was gathered from international contributions (Table 1). The US program GO-BGC provided 5 units, the Canadian program Argo-Canada provided 4 units, the Principality of Monaco donated 1 unit to Seychelles and 1 unit to Mauritius,

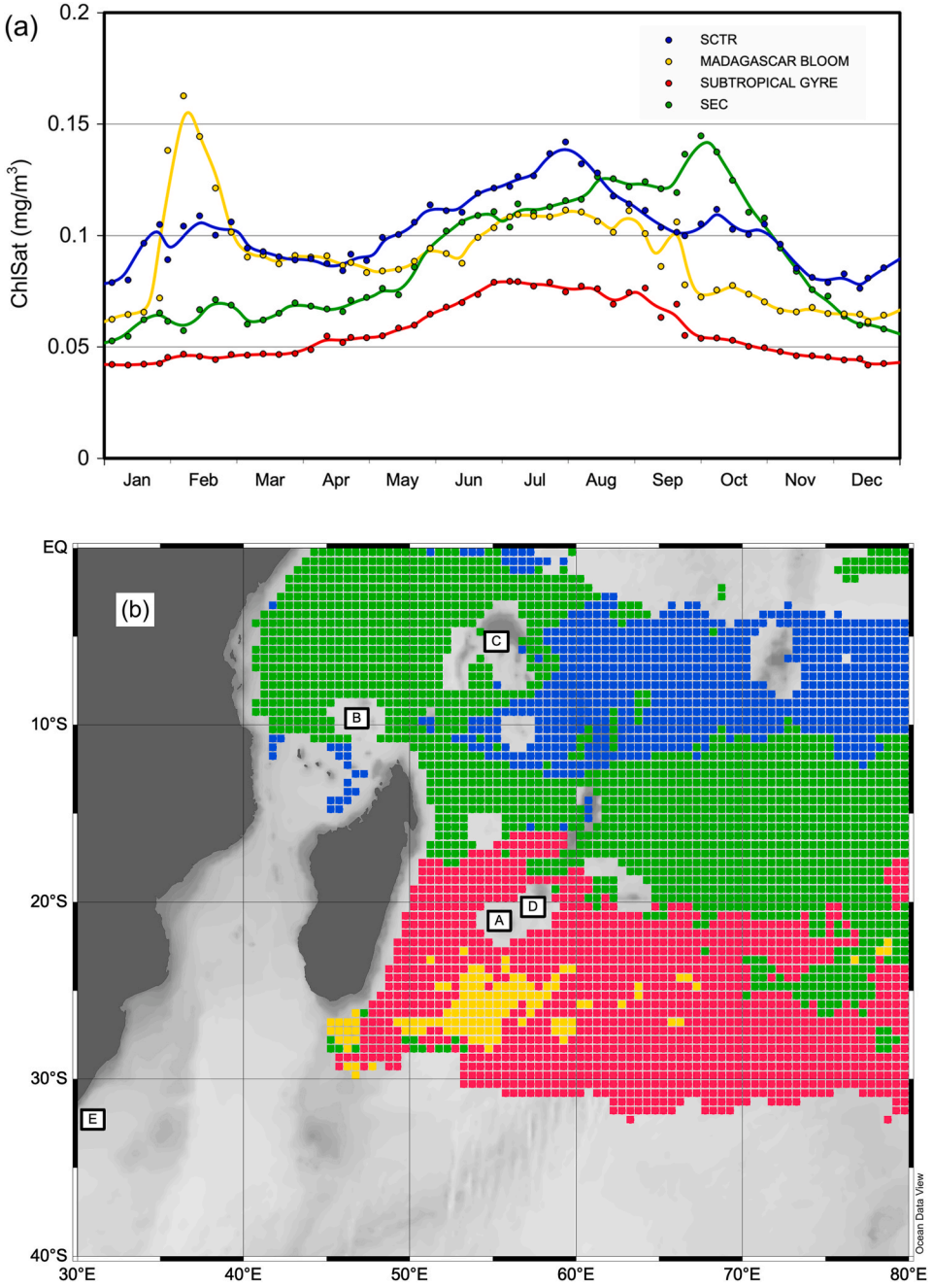

Fig. 2. a) mean ChlSat seasonal cycles in the four bioregions; b) spatial extension of the bioregions. The 5 ports of call planned for the ME-IO expedition are indicated: La Réunion (A), Aldabra (B), Mahé (C), Mauritius (D), Cape Town (E).

the European project ERC REFINE provided 3 units, and the French project Equipex NAOS provided 3 units.

A specific deployment strategy was set up in order to cover the biogeochemical contrasts in the SWIO. Indicators of such contrasts were sketched from the distribution of the water masses (Section 3.1). As access to deep nutrient pools influences phytoplankton productivity, nitrate supply into the sunlit layer can be inferred by the depth and the thickness of the nitracline. In a latitudinal perspective (Fig. 1g), the shape of the nitracline is intrinsically associated to the distribution of CW and leads to contrasted situations: sharper and shallower nitraclines in the SCTR than in the subtropical gyre and the Mascarene Bowl. Noteworthy, the surface nutrient-rich waters carried by the SEC would provide a horizontal supply into the Mascarene and Somali Basins.

In order to refine the deployment strategy at the scale of the ME-IO cruise transects, a bioregionalization based on phytoplanktonic seasonal cycles was applied to the SWIO (following Huot et al., 2019; Supplementary Material C). The obtained partition delineates areas of similar surface chlorophyll seasonality (Figure C2) that match with the extensions of the SCTR, the SEC, and of the subtropical gyre north of 35°S (Fig. 1a). Combining the latitudinal patterns of nutrient supply with this bioregionalization: i) SCTR was differentiated with the subtropical gyre, ii) the isolated parcels embedded in the zone of influence of the SEC were assembled with the encompassing bioregion.

This analysis led to a compilation of four bioregions with distinct ChlSat seasonal cycles (Fig. 2). The spatial signature of the SCTR (Fig. 2, in blue) is identifiable as a standalone band east of 55°E and between 3°S and 10°S. Its seasonal cycle is characterized by a winter increase of chlorophyll concentration to 0.14 mg m^{-3}. During the rest of the year, the baseline remains below 0.10 mg m^{-3} with another peak of lower magnitude mid-summer. In the areas influenced by the SEC and its northeastward extension (Fig. 2, in green), seasonality is marked: ChlSat almost triple between summer and winter peaking near 0.15 mg m^{-3} in early spring. The subtropical gyre (Fig. 2, in red) presents a stable ChlSat concentration limited around 0.05 mg m^{-3} all year long. The Madagascar bloom bioregion (Fig. 2, in yellow) is wrapped inside the subtropical gyre. The seasonal course of ChlSat presents a peak during summer, then it is damped to the cycle of the subtropical gyre (Longhurst, 2001; Uz, 2007; Srokosz and Quartly, 2013; Lévy et al., 2007; Srokosz et al., 2015; Dilmahamod et al., 2019; Huhn et al., 2012; Metzl et al., 2022).

In association with bioregions, a Lagrangian analysis was conducted from historical Argo trajectories (Supplementary Material D). This approach estimated a mean residence time in each bioregion and their degree of interconnectivity (Table 2). The SCTR and SEC bioregions have limited retention times, with respectively seven and eight months; they display strong interconnectivity with two-way exchanges of almost 40 % of floats. In the subtropical gyre, mean retention time increases to almost one year and the main export pathways are steered into the Mozambique and Crozet Basins.

Overall, the deployment strategy was set up on the basis of the preliminary cruise track (four transects joining the marks A-E, Fig. 2b), the number of available floats, the expected biogeochemical contrasts defined by four bioregions, and a quantitative estimation of residence times and connectivity pathways. The provisional plan of deployment consisted in a suite of oceanographic stations in the high seas (some in the national jurisdictions of the Seychelles, Mauritius and France) to be occupied during the ME-IO expedition. A number of BGC-Argo floats to be deployed was assigned to every stations.

- The transect A-B would cross the inner Mascarene Basin in the subtropical gyre and along the SEC: one station northwest of La Réunion (2 units), one station in SEC (2 units), one station northeast of Madagascar (1 unit).
- The transect B-C would cross the Somali Basin: one station northeast of Aldabra (2 units), one station southwest of Mahé (2 units).
- The transect C-D along the Mascarene Arc would cross the SCTR and the upstream part of the SEC: one station southeast of Mahé (3 units), one station in SEC (1 unit), one station northeast of Mauritius (1 unit).
- The transect D-E would cross the Madagascar and Mozambique Basins in the region of the Madagascar Bloom: three stations were displayed at the southeastern tip of Madagascar at three parallels (25°S, 27°30′S, 30°S, 3 units).

Table 2
Mean residence time of an Argo float inside every bioregion and fraction exported in the neighboring bioregion or outside the SWIO. Seychelles Chagos Thermocline Ridge (SCTR), South Equatorial Current (SEC), subtropical gyre (STG), Madagascar Bloom (MB).

bioregion	mean residence time (in days)	interconnectivity (in %)			
		SCTR	SEC	STG + MB	outside
SCTR	206	14	39	–	47
SEC	233	37	15	23	25
STG + MB	355	–	27	21	52

4. ME-IO deployments and outcomes

In spring 2022, the ME-IO expedition surveyed a large latitudinal band of the SWIO, crossing the Mozambique and Madagascar Basins, heading north in the Mascarene Basin, entering the Tropical band by the Amirante Trough and heading east from Comoros to Seychelles, then heading south to Mauritius along the Mascarene Arc, and finally returned to Cape Town. Along this path, seventeen BGC-Argo floats were successfully deployed at twelve oceanographic stations (Fig. 3a). The oceanic regimes and biogeochemical conditions crossed by the ME-IO expedition during the Austral springtime 2022 are reported in Sections 4.1 and 4.2. In Section 4.3, two years of operations of the BGC-Argo array allowed to describe contrasted phytoplanktonic seasonal cycles and underlying biophysical interactions. Collected data from the station located inside the Mozambique Basin are considered only through Section 4.1. In relation to its trajectory, data collected by the float deployed there was not considered.

4.1. Oceanic regimes crossed by the ME-IO expedition

Twelve reference oceanographic stations associated with deployments of BGC-Argo floats were occupied during the ME-IO expedition. The collected hydrographic records allowed to classify these stations following the oceanic regimes described in Section 3.1. Looking at the temperature-salinity diagram (Fig. 3b), four sets of profiles can be differentiated thanks to the composition of intermediate waters (density classes larger than 26.8): AAIW at high latitudes progressively mixing with RSOW at low latitudes. Considering Central Water (density class 24.8–26.8), two groups appear separated by the transition between the subtropical gyre and the tropical band (respectively regions 3–4 and regions 1–2). Looking now at the nitrate-density diagram (Fig. 3c), differences between stations occur in the nitrate concentration of the CW (density class 24.8–26.8). It is almost nitrate-depleted in the high latitudes (region 4), and it becomes slightly enriched, reaching up to 4 μmolN·kg^{-1} in region 3. On the other hand, in regions 1 and 2, nitrate concentrations remain high in CW, but values sharply decrease to zero inside the surface layer.

The easternmost station of region 2 located within the Mascarene Arc, south of Saya de Malha bank (at 13°S, 60°E) presents the lowest salinity and the highest nitrate concentration of the region. This signature attests of the SEC supply of fresh an rich water (New et al., 2005).

Overall, a correspondence can be done between every region sampled by the cruise and oceanic regimes of the SWIO. North of 15°S, the classification identifies the SCTR with region 1 (in blue) and the SEC with region 2 (in green). South of 15°S in the subtropical gyre, the

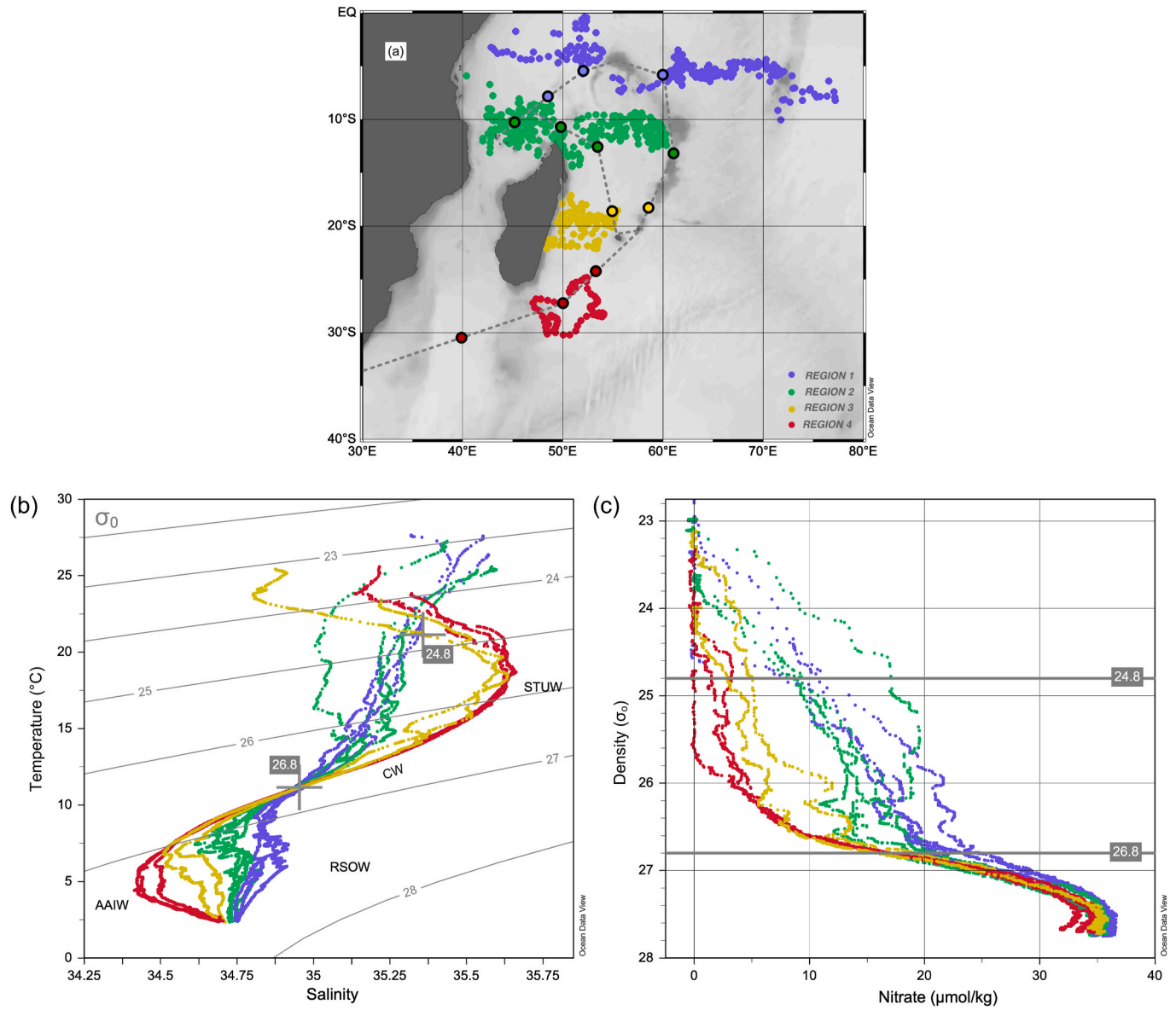

Fig. 3. a) Ship track of the ME-IO expedition and location of float deployments (colour dots circled in black). The profile locations of floats during the two following years are also indicated (colour dots) as reported in Table 1 b) temperature-salinity diagram of the twelve CTD casts. c) nitrate-density diagram the twelve CTD casts. Isopycnals are shown as contours; gray crosses and lines indicate the isopycnals 24.8 and 26.8. The colours of dots and profiles correspond to regions 1 to 4 respectively in blue, green, yellow and red. (For interpretation of the references to colour in this figure legend, the reader is referred to the Web version of this article.)

classification distinguishes the Mascarene bowl (region 3, in yellow) with the inner subtropical gyre (region 4, in red). The locations of the four sets of stations occupied during the cruise (Fig. 3a) notably match with the bioregions (Fig. 2b).

4.2. Contrasted biogeochemical conditions

A springtime snapshot of the biogeochemical conditions in the SWIO was drawn using the reference dataset collected during the ME-IO expedition (Fig. 4a). During this season, the vertical distribution of biomass systematically displayed a DCM for all regions. This DCM varied in depth and size between regions: it was shallower and more pronounced in region 1, then progressively deepened and widened toward the southernmost regions. Surface values of biomass were significantly lower in the subtropical regions (3 and 4) than in the tropical regions (1 and 2).

The nutrient supply in the sunlit layer could explain such distribution of biomass: it does not affect phytoplankton production in the tropical regions, whereas it is a limitation in the subtropical regions. The shape of the nitracline is sharp and shallow within the sunlit layer for regions 1 and 2, whereas, in regions 3 and 4, it is more gradual leaving the sunlit layer nitrate-depleted. Overall, in this springtime situation, phytoplanktonic production followed distinct regimes: in the tropical band, nutrient-rich waters are upwelled into a relatively shallow surface layer that embeds biological activity. In the subtropical gyre, the surface layer is depleted in nutrients and phytoplankton biomass is concentrated at a depth which guarantees optimal availability of nutrient supply and light for its growth.

Interestingly, for most of the oceanographic stations visited during the cruise, the isopycnal 24.8 is indicative of the top of nitracline (gray dashed lines in Fig. 4a). This matchup was particularly marked in regions 1 and 2. This isopycnal corresponds to the base of the nutrient-depleted layer in regions 3 and 4 as the nitrate gradient is smoother there. This is in agreement with the nitrate-density diagram presented in

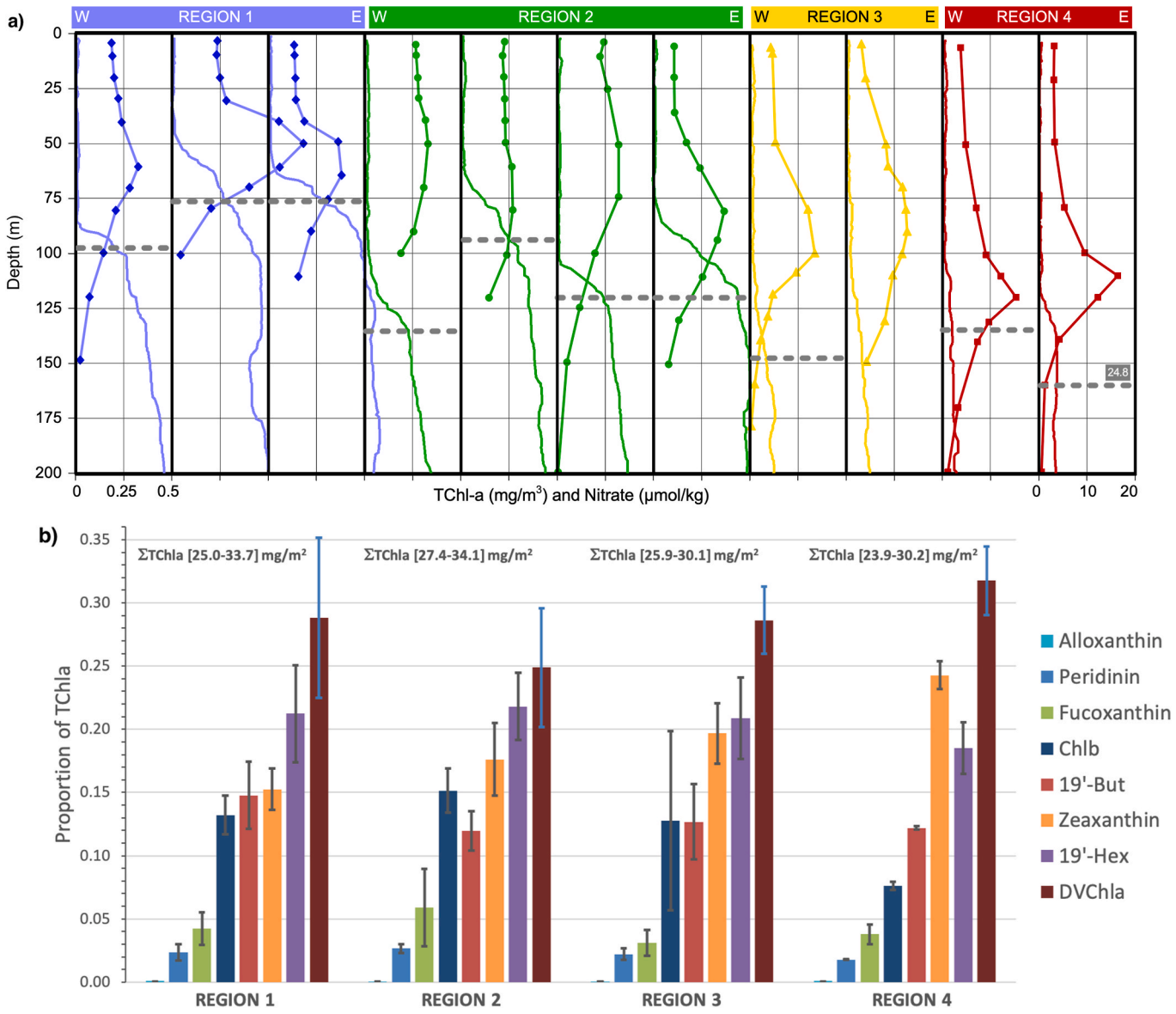

Fig. 4. a) profiles of Total Chlorophyll-a measured by HPLC (thick dotted lines) and nitrate concentrations (continuous thin line) at the eleven CTD casts of the ME-IO expedition north of 30°S. The depth of isopycnal 24.8 is indicated in horizontal dashed gray lines. Profiles are classified by region and ordered from west to east. b) regional average and standard deviation of profiles collected in every region, proportion of significant pigments (integrated in the HPLC profile) as normalized by integrated TChl-a (range reported on above each bar).

Fig. 4c, where this isopycnal marks the top of the CW and the beginning of the permanent thermocline. As described previously, in Section 3.1, the Mascarene Bowl deepens the CW and blocks the nitrate supply in the surface layer. Biological activity in region 3 should be reduced as a consequence, especially in comparison with that of region 4. On the other hand, the SEC brings nutrient-rich waters into the surface water layer enhancing biological activity in both regions 2 and 3.

The integrated biomass measurements show little variation between the regions, with internal regional differences in Total Chlorophyll-a being more pronounced than inter-regional gaps. (Fig. 4b). Phyto-plankton pigments assemblages can be indicative of the phytoplankton community encountered. In the four defined regions, DVChl-a dominates the pigment assemblage comprising over 25 % of TChl-a, followed by 19′-Hex and zeaxanthin, suggesting a community rich in nano- and pico-plankton (e.g., prochlorophytes, cyanobacteria, prymnesiophytes). Region 4 stands out with over 50 % representation of DVChl-a and zeaxanthin, indicating a higher prevalence of pico-plankton, while showing a decline in prymnesiophyte. In this region, and contrary to the three other regions, 19′-Hex-containing species contribute less than Zeaxanthin-containing species to TChl-a, indicating a decrease in prymnesiophytes cell number. On the other hand, the small proportion of peridinin and fucoxanthin may indicate the low abundance of larger cells such as dinoflagellates or diatoms.

Overall, phytoplankton exhibit significant variation in abundance and type across different water bodies (Fogg and Thake, 1987). The patterns observed in our results align with the general concept of phytoplankton distribution. The nutrient supply in the sunlit layer can help explain this biomass distribution: in tropical regions, nutrient in-jection by upwellings and the SEC foster biological activity dominated by nano- and pico-plankton, whereas nutrient availability becomes a limiting factor in subtropical areas.

4.3. *Phytoplanktonic seasonal cycles*

The observation of the springtime biogeochemical conditions can be extended over time thanks to the array of autonomous sensors deployed

during the cruise. In order to inspect seasonal changes, a subset of BGC-Argo floats was selected according to their dispersion in the four regions of interest (Fig. 3a). For the sake of metrological consistency, each selected float sampled a sole region during at least one year. Overall, twenty-four annual time series were extracted from the data collected by the thirteen BGC-Argo floats (Table 1).

The seasonal evolution of Chl-a fluorescence in the upper 250 m could be documented in every region (Fig. 5, lower panel). The DCM-shape characterized during the ME-IO cruise was reproduced during the whole year with significant modulations in amplitude, depth, and size. Mixing episodes, proxied by MLD deepening during winter, dampen the DCM signature as phytoplankton biomass is dispersed toward the surface. These events were longer in regions 1 and 2 (from July to September) than in region 4 (only during August), as also documented in the seasonal courses of surface Chl-a (Fig. 5, middle panels). However, these seasonal modulations were moderately reflected into the course of integrated Chl-a (Fig. 5, upper panels) that remained in the range of 20–35 mg m^{-2} for all regions.

In order to characterize such changes in the phytoplanktonic dynamics, biophysical interactions were analyzed with respect to the seasonal course of the MLD and the isopycnal 24.8 (Fig. 4, bottom panels). Chosen as a proxy of the nitracline, the isopycnal 24.8 would mark the decline of nitrate in the sunlit layer in the tropical band (regions 1 and 2), whereas in the subtropical gyre (regions 3 and 4), this isopycnal would sign the top of the nitrate reservoir. Such correspondence between isopycnal 24.8 and the nitracline can be consolidated in the view of nitrate time series collected by individual BGC-Argo floats (Supplementary Material B).

In region 1, the isopycnal 24.8 was located 20 m below the DCM and remained shallow in winter as well in summer. The isopycnal 24.8 quickly deepened in July, the DCM remained shallow and slowly decayed by the end of winter. The course of surface Chl-a followed with the mixed layer depth which deepened down to 40 m in summer and in winter, without reaching the DCM. Compensating effects of both MLD and isopycnal 24.8 deepening (less access to nitrate but more access to light) would have maintained the phytoplankton ecosystem during the whole winter. Same results were magnified in region 2. There, the isopycnal 24.8 was on average deeper than in region 1, and dropped down to 150 m at the end of winter. The MLD also reached deeper levels (down to 60 m) during the whole winter. The DCM was slightly deeper in this region but reached the mixed layer during winter.

In region 3, the phytoplankton dynamics was stable during the year, because of the limited access to nutrients. The DCM remained at 100 m depth, whereas the isopycnal 24.8 remained 75 m below. The MLD varied between 20 m in summer and 60 m in winter. In this season, part of the phytoplankton biomass was entrained in the mixed layer associated to a slight increase in the surface Chl-a. The nutrient barrier was relaxed in the region 4, the DCM and the isopycnal 24.8 were both located at 75 m depth. The DCM followed a summer deepening and winter shallowing associated to seasonal sunlight variations. The MLD increased in winter down to 70 m depth then shallowed at the beginning of spring, triggering a phytoplankton bloom that rapidly decayed in absence of nutrient supply.

Overall, the nitrate supply was limited in the subtropical gyre where oligotrophic conditions were installed all year long. Such conditions were reinforced by the Mascarene Bowl which deepened the nitracline away from the sunlit layer. These hydrodynamical conditions were released more south, and combined with sharper winter conditions that extended at depth the seasonal excursion of the mixed layer, occasional spring blooms could occur. Nutrient limitation was released in the tropical band: upwelling conditions persisted during the whole year, even if seasonal modulations were observed in association with changes

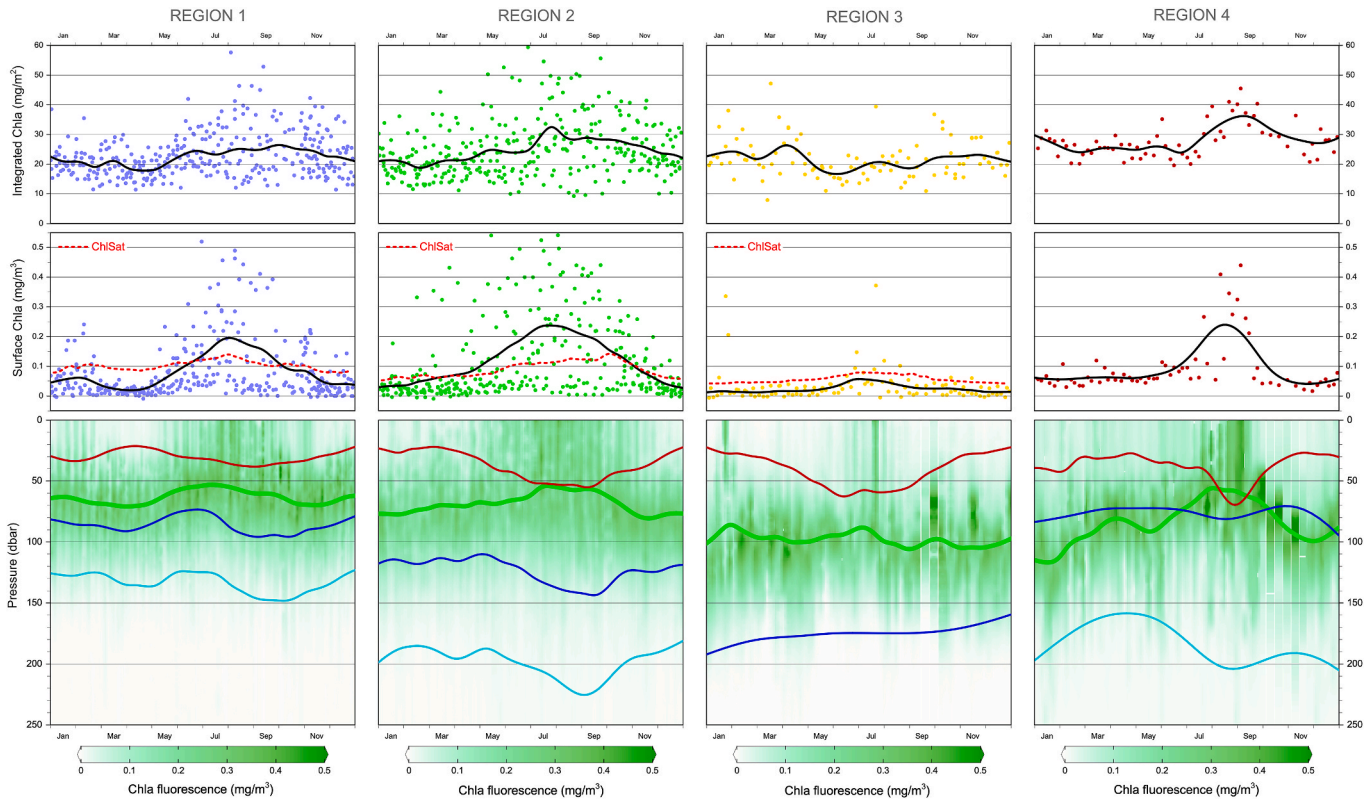

Fig. 5. Average seasonal cycle of each region as seen by the BGC-Argo dataset. Upper panels: depth-integrated Chl-a estimated by fluorescence. Middle panel: surface Chl-a estimated by fluorescence. Lower panel: Chl-a fluorescence profiles (colourbar), mixed layer depth (MLD, red lines), deep chlorophyll maximum (DCM, green lines), depth of isopycnal 24.8 (blue line), and depth of isopycnal 26.0 (cyan line). (For interpretation of the references to colour in this figure legend, the reader is referred to the Web version of this article.)

in the thermocline depth and stratification.

5. Discussion

During the ME-IO expedition, we deployed seventeen BGC-Argo floats across twelve oceanographic stations. Thanks to the deployment strategy, the float array effectively sampled the large scale biophysical regimes of the SWIO collecting more than 1000 profiles. With only one faulty unit and three profilers drifting away from their targeted sampling zones, thirteen floats remain operational in the region. Despite a clear signature in preliminary analyses and targeted deployment stations, the Madagascar bloom was not sampled by the BGC-Argo array.

Collected data offer exceptional insight into the underlying mechanisms driving the subsurface bio-physical processes and consequently phytoplankton seasonality in the SWIO. These observations extended the ME-IO expedition sampling and complemented the space borne description of the tropical band seasonality (Lévy et al., 2007; Resplandy et al., 2009; Aguiar-González et al., 2016; George et al., 2018, Section 3.2). The role of circulation in regulating access to nutrient, hence shaping productivity, is particularly highlighted within the Mascarene bowl.

The SCTR exhibits strong sensitivity to climatic variability (Resplandy et al., 2009; Dilmahamod et al., 2016; Lee et al., 2022; Yamagata et al., 2024), with documented implications for regional fisheries (Robinson et al., 2010; Kim and Na, 2022; Marsac et al., 2024). Given its significance, sustained, zonally resolved observations of this region with Argo and BGC-Argo floats is a priority (IndOOS-2 Full Report, 2019). Due to currents, continuous deployment efforts are essential in maintaining observational coverage of the SEC. In contrast, float retention is expected to be higher within the subtropical gyre, thereby reducing the servicing demands. However, over the Madagascar Ridge located at the southern tip of the island, dynamic southwestward pathways carried three floats towards the African coast (Vianello et al., 2020). Consequently, targeted field campaigns may offer a more effective approach to resolve the drivers of the Madagascar bloom. In the subtropical band, Read et al. (2000) highlighted that nitrate is not the limiting factor for phytoplankton growth. Therefore, any extrapolation of the described subtropical gyre dynamics, should be limited to regions north of 30°S.

The partitioning of the SWIO into bio-physical regimes is coherent seen from satellite and with the BGC-Argo float array. Applying the same frame at finer ecological scales becomes more delicate. Our *in-situ* data emphasize the role of the nano- and pico-phytoplankton compartment in the biomass production of these tropical and subtropical areas. Nevertheless, pigment data also suggest a predominant role of prokaryotes in exploiting these low nutrient conditions and driving primary production. Brock et al., 2024have shown that two clades of Prochlorococcus dominated the microbial community in the Indian Ocean. In our study, cell counts by microscopy as well as flow cytometry data could help assess the spatial heterogeneity of eukaryotic and bacterial communities. The effect of environmental drivers of each region could then be associated with a diversity shift. DNA sequencing and taxonomic assignment would also enhance our understanding of biodiversity and connect it with the physical and chemical properties of the studied regions. Hence, combining the discrete sampling from the ME-IO expedition with bio-optical measurements (e.g., fluorescence chlorophyll-a and backscattering coefficient) from the BGC-Argo float time series will help establish specific relationships to gain a deeper understanding of the dynamics of phytoplankton communities and their interactions with grazing and larger predators, as highlighted by Rembauville et al. (2017) for other oceanic regions.

Numerical models provide a powerful framework to address observational gaps. These models also facilitate the integration of interconnected domains, coupling natural (physical oceanography, biogeochemistry, and trophic levels) and human systems (fisheries and broader socio-ecological systems). The biogeochemical measurements collected by the deployed float array represent a foundational dataset, essential for the development of coupled model simulations (Hermes et al., 2019; Schwarz, 2020).

6. Conclusion

This study presents the experimental strategy followed to set-up an array of BGC-Argo floats in the SWIO, the outcomes of its deployment after two years of operations, and guidelines for future initiatives.

To design a regional array of biogeochemical floats, the deployment strategy was grounded on past experiences, existing knowledge, and the analysis of historical datasets. First, we identified areas of contrasted oceanic regimes and biogeochemical conditions to be covered by the array: the tropical band with productive upwellings associated to the Seychelles Chagos Thermocline Ridge, the band overlaying the South Equatorial Current, and the subtropical gyre. Second, we assessed the residence times inside each potential deployment zone using historical float trajectories. Third, we selected deployment stations along the provisional track of the expedition on the basis of the number of floats. The resulting array covers the three biophysical regimes, with denser float distribution north of 15°S, aligning with IndOOS-2 recommendations to enhance biogeochemical observations in productive areas.

Following this strategy, a fleet of 17 biogeochemical floats has been successfully deployed during the expedition in October–November 2022. The data collection gathers physical (temperature, salinity), chemical (oxygen, pH, nitrate) and optical (chlorophyll fluorescence, backscattering, irradiance) seawater properties as continuous vertical profiles in the upper 2 km. In-situ metrological verification of the autonomous sensors and data quality control could be achieved at float deployments concomitantly to ship-borne reference measurements.

After two years of operations, the spatio-temporal distribution covered by the fleet confirmed that the goals of the deployment strategy have been reached. The observing system allowed to describe a variety of oceanic regimes, circulation features and associated biogeochemical conditions over the SWIO. As shown by the deployed BGC-Argo float array, the physical-biogeochemical functioning is strongly controlled by the distribution of water masses which stratification regulates the access to nutrients. Seasonal variations in nutrient supply, thermocline depth, and stratification drive the tropical band productivity with year-round upwelling conditions. In the subtropical gyre, nutrient barriers associated to subduction of depleted subtropical water masses, limit further productivity. Oligotrophic conditions persist due to nutrient depletion by surface recirculation, although occasional spring blooms occur after intense enough mixing events.

While the results presented here are still preliminary, they demonstrate the vast potential of a globally coordinated, dense, and continuously maintained BGC-Argo array in supporting science and resilient regional governance.

CRediT authorship contribution statement

Wilhem Riom: Writing – original draft, Investigation. **Vincent Taillandier:** Writing – original draft, Methodology, Investigation, Formal analysis, Data curation, Conceptualization. **Céline Dimier:** Formal analysis, Data curation, Writing – original draft, Investigation. **Fabrizio D'Ortenzio:** Writing – original draft, Funding acquisition, Conceptualization. **Hervé Claustre:** Supervision, Funding acquisition.

Data availability

Data collected by the array of profiling floats were made freely available by the international Argo program and the national programs that contribute to it (Argo, 2000; https://doi.org/10.17882/42182). The Argo Program is part of the Global Ocean Observing System. In-situ data collections of the ME-IO expedition, composed of post-cruise quality controlled CTD profiles and laboratory measurements, are

freely available (Taillandier et al., 2024; https://doi.org/10.17882/98833). Satellite data were collected from the OCEANCOLOUR_GLO_BGC_L3_MY_009_103 product, provided by the Copernicus Marine Environment Monitoring Service (CMEMS, http://marine.copernicus.eu/). Historical float trajectories were extracted the Profile directory file and the Synthetic-Profile directory file of the Argo Global Data Assembly Center (https://data-argo.ifremer.fr/) accessed in April 2025.

Declaration of generative AI and AI-assisted technologies in the writing process

During the preparation of this work the authors used ChatGPT-4 from OpenAI (https://chat.openai.com) in order to improve the readability and language of the manuscript. After using this tool/service, the authors reviewed and edited the content as needed and take full responsibility for the content of the publication.

Funding sources

The authors of this study acknowledge the financial supports of the project REFINE (European Research Council, Grant agreement 834177), the project Equipex + Argo-2030 (grant ANR-21-ESRE-0019) and the project BRIDGES-AVATAR (grant ANR-22-EXBR-0004); the two latter are integrated in France (2030) and managed by Agence Nationale de la Recherche. The phytoplankton pigment analyses were performed at the SAPIGH national HPLC analytical service at the Institut de la Mer de Villefranche (IMEV), France. WR received support from the CNES/TOSCA project SEASONS.

Declaration of competing interest

The authors declare the following financial interests/personal relationships which may be considered as potential competing interests: Wilhem Riom reports article publishing charges were provided by Explorations de Monaco/Monaco Explorations. Vincent Taillandier, Céline Dimier, Fabrizio D'Ortenzio and Hervé Claustre report travel charges were provided by Explorations de Monaco/Monaco Explorations. If there are other authors, they declare that they have no known competing financial interests or personal relationships that could have appeared to influence the work reported in this paper.

Acknowledgements

The authors of this study would like to express their thanks and gratitude towards Monaco Explorations (www.monacoexplorations.org) for the coordination and funding of the Indian Ocean expedition 2022 , the S.A. Agulhas II officers and crew members for their assistance during the cruise, Thomas Jessin and Antoine Poteau for their help on the preparation and the deployment of the floats, Louis Prieur and Jean-François Ternon for their precious comments and preliminary discussions.

Authorisations granted for the scientific work are as follows: For research conducted in Saya de Malha : As per the Memorandum of Understanding between Monaco Explorations and the designated authority of the joint management area signed on 13/06/2022; For research conducted in Mauritius ZEE : As per the Memorandum of Understanding between Monaco Explorations and Prime Minister's office, Departement for continental shelf, maritime zones administration and exploration signed on 13/06/2022 ; For research conducted in Seychelles ZEE : As per the Memorandum of Understanding between Monaco Explorations and the Seychelles Government signed on 14/10/2022 ; For research conducted in the French ZEE : As per the note of the French Ministry for Europe and Foreign Affairs issued on 19/08/2022.

Appendix A. Supplementary data

Supplementary data to this article can be found online at https://doi.org/10.1016/j.dsr2.2025.105504.

Data availability

Data will be made available on request.

References

Aguiar-González, Borja, Ponsoni, Leandro, Ridderinkhof, Herman, Van Aken, Hendrik M., De Ruijter, Will P.M., Maas, Leo R.M., 2016. Seasonal variation of the South Indian tropical gyre. Deep Sea Res. Oceanogr. Res. Pap. 110, 123–140. https://doi.org/10.1016/j.dsr.2016.02.004.

Ahmed, Mohiuddin, Seraj, Raihan, Islam, Syed Mohammed Shamsul, 2020. The K-means algorithm: a comprehensive survey and performance evaluation. Electronics 9 (8), 1295. https://doi.org/10.3390/electronics9081295.

Ardyna, Mathieu, Claustre, Hervé, Sallée, Jean-Baptiste, D'Ovidio, Francesco, Gentili, Bernard, Van Dijken, Gert, D'Ortenzio, Fabrizio, Arrigo, Kevin R., 2017. Delineating environmental control of phytoplankton biomass and phenology in the Southern Ocean. Geophys. Res. Lett. 44 (10), 5016–5024. https://doi.org/10.1002/2016GL072428. May 28.

Argo, 2000. Argo Float Data and Metadata from Global Data Assembly Centre (Argo GDAC). SEANOE. https://doi.org/10.17882/42182.

Baudena, Alberto, Riom, Wilhem, Vincent, Taillandier, Mayot, Nicolas, Mignot, Alexandre, D'Ortenzio, Fabrizio, 2025. Comparing satellite and BGC-argo chlorophyll estimation: a phenological study. Remote Sens. Environ. 326, 114743. https://doi.org/10.1016/j.rse.2025.114743.

Beal, L.M., Vialard, J., Roxy, M.K., Li, J., Andres, M., Annamalai, H., Feng, M., et al., 2020. A road map to IndOOS-2: better observations of the rapidly warming Indian ocean. Bull. Am. Meteorol. Soc. 101 (11), E1891–E1913. https://doi.org/10.1175/BAMS-D-19-0209.1.

Biogeochemical-Argo Planning Group, 2016. *The Scientific Rationale, Design And Implementation Plan For a Biogeochemical-Argo Float Array*. Pdf. Ifremer. https://doi.org/10.13155/46601.

Bittig, Henry C., Maurer, Tanya L., Plant, Joshua N., Schmechtig, Catherine, Wong, Annie P.S., Claustre, Hervé, Trull, Thomas W., et al., 2019. A BGC-argo guide: planning, deployment, data handling and usage. Front. Mar. Sci. 6 (August 22), 502. https://doi.org/10.3389/fmars.2019.00502.

Brock, Melissa L., Larkin, Alyse A., Raes, Eric J., Martiny, Adam C., 2024. Bacterial biogeography of the Indian ocean. Limnol. Oceanogr. 69 (1), 67–80. https://doi.org/10.1002/lno.12459.

Chai, Fei, Johnson, Kenneth S., Claustre, Hervé, Xing, Xiaogang, Wang, Yuntao, Boss, Emmanuel, Riser, Stephen, Fennel, Katja, Schofield, Oscar, Sutton, Adrienne, 2020. Monitoring Ocean biogeochemistry with autonomous platforms. Nat. Rev. Earth Environ. 1 (6), 315–326. https://doi.org/10.1038/s43017-020-0053-y. May 21.

Chassot, Emmanuel, Bonhommeau, Sylvain, Dulvy, Nicholas K., Mélin, Frédéric, Watson, Reg, Gascuel, Didier, Olivier, Le Pape, 2010. Global marine primary production constrains fisheries catches. Ecol. Lett. 13 (4), 495–505. https://doi.org/10.1111/j.1461-0248.2010.01443.x.

Claustre, Hervé, Johnson, Kenneth S., Takeshita, Yuichiro, 2020. Observing the Global Ocean with biogeochemical-argo. Ann. Rev. Mar. Sci 12 (1), 23–48. https://doi.org/10.1146/annurev-marine-010419-010956. January 3.

Coopen, Priscilla, Yuneeda, B., Oozeeraully, N., Ostrowski, Marek, 2022. Ocean Circulation over the Saya de Malha Bank in the South West Indian Ocean. West. Indian Ocean J. Mar. Sci. (2), 1–13. https://doi.org/10.4314/wiojms.si2021.2.1, 2021 (July 20.

Coppola, Laurent, Diamond Riquier, Emilie, Carval, Thierry, , Jean-Olivier Irisson, Desnos, Corinne, 2024. Dyfamed Observatory Data. SEANOE. https://doi.org/10.17882/43749.

Dalpadado, Padmini, Roxy, Mathew Koll, Arrigo, Kevin R., Van Dijken, Gert L., Chierici, Melissa, Ostrowski, Marek, Skern-Mauritzen, Rasmus, Bakke, Gunnstein, Richardson, Anthony J., Sperfeld, Erik, 2024. Rapid climate change alters the environment and biological production of the Indian ocean. Sci. Total Environ. 906, 167342. https://doi.org/10.1016/j.scitotenv.2023.167342.

Dexter, Peter, Summerhayes, Colin, 2010. 11 Ocean Observations: the Global Ocean Observing System.

Dilmahamod, A.F., Penven, P., Aguiar-González, B., Reason, C.J.C., Hermes, J.C., 2019. A new definition of the South-east Madagascar bloom and analysis of its variability. J. Geophys. Res.: Oceans 124 (3), 1717–1735. https://doi.org/10.1029/2018JC014582.

Dilmahamod, A.F., Hermes, J.C., Reason, C.J.C., 2016. Chlorophyll-a variability in the Seychelles–Chagos Thermocline Ridge: analysis of a coupled biophysical model. J. Mar. Syst. 154, 220–232. https://doi.org/10.1016/j.jmarsys.2015.10.011.

D'Ortenzio, F., Ribera d'Alcalà, M., 2009. On the trophic regimes of the Mediterranean Sea: a satellite analysis. Biogeosciences 6 (2), 139–148. https://doi.org/10.5194/bg-6-139-2009. February 5.

D'Ortenzio, Fabrizio, Antoine, David, Martinez, Elodie, Ribera d'Alcalà, Maurizio, 2012. Phenological changes of oceanic phytoplankton in the 1980s and 2000s as revealed by remotely sensed ocean-color observations. Glob. Biogeochem. Cycles 26 (4), 2011GB004269. https://doi.org/10.1029/2011GB004269.

D'Ortenzio, Fabrizio, Iudicone, Daniele, De Boyer Montegut, Clement, Testor, Pierre, Antoine, David, Marullo, Salvatore, Santoleri, Rosalia, Madec, Gurvan, 2005. Seasonal variability of the mixed layer depth in the Mediterranean Sea as derived from in situ profiles. Geophys. Res. Lett. 32 (12), 2005GL022463. https://doi.org/10.1029/2005GL022463.

D'Ortenzio, Fabrizio, Vincent, Taillandier, Claustre, Hervé, Prieur, Louis Marie, Leymarie, Edouard, Mignot, Alexandre, Poteau, Antoine, Penkerc'h, Christophe, Schmechtig, Catherine Marie, 2020. Biogeochemical Argo: the test case of the NAOS mediterranean array. Front. Mar. Sci. 7 (March 24), 120. https://doi.org/10.3389/fmars.2020.00120.

Fine, Rana A., 1993. Circulation of antarctic intermediate water in the South Indian ocean. Deep Sea Res. Oceanogr. Res. Pap. 40 (10), 2021–2042. https://doi.org/10.1016/0967-0637(93)90043-3.

Fogg, G.E., Thake, B., 1987. Algal Cultures and Phytoplankton Ecology.

Freeland, Howard, 2007. A short history of ocean station Papa and line P. Prog. Oceanogr. 75 (2), 120–125. https://doi.org/10.1016/j.pocean.2007.08.005.

"Full Report, 2019. IndOOS-2: A Roadmap to Sustained Observations of the Indian Ocean for 2020-2030. CLIVAR. https://doi.org/10.36071/clivar.rp.4.2019. December 10.

George, Jenson V., Nuncio, M., Anilkumar, N., Chacko, Racheal, Rajashekhar, D., 2018. Seasonal surface chlorophyll a variability in the Seychelles–Chagos Thermocline Ridge. Curr. Sci. 114 (4), 868. https://doi.org/10.18520/cs/v114/i04/868-878.

Groom, Steve, Sathyendranath, Shubha, Ban, Yai, Stewart, Bernard, Brewin, Robert, Brotas, Vanda, Brockmann, Carsten, et al., 2019. Satellite Ocean colour: current status and future perspective. Front. Mar. Sci. 6 (August 29), 485. https://doi.org/10.3389/fmars.2019.00485.

Guo, Mingxian, Peng, Xiu, Xing, Xiaogang, 2022. Oceanic fronts structure phytoplankton distributions in the central south Indian ocean. J. Geophys. Res.: Oceans 127 (1), e2021JC017594. https://doi.org/10.1029/2021JC017594.

Hartigan, J.A., Wong, M.A., 1979. Algorithm as 136: a K-means clustering algorithm. Applied Statistics 28 (1), 100. https://doi.org/10.2307/2346830.

Hermes, J.C., Masumoto, Y., Beal, L.M., Roxy, M.K., Vialard, J., Andres, M., Annamalai, H., et al., 2019. A sustained Ocean Observing system in the Indian ocean for climate related scientific knowledge and societal needs. Front. Mar. Sci. 6 (June 28), 355. https://doi.org/10.3389/fmars.2019.00355.

Hermes, J.C., Reason, C.J.C., 2008. Annual cycle of the South Indian ocean (Seychelles-Chagos) Thermocline Ridge in a regional ocean model. J. Geophys. Res.: Oceans 113 (C4). https://doi.org/10.1029/2007JC004363, 2007JC004363.

Hernández-Guerra, Alonso, Talley, Lynne D., 2016. Meridional overturning transports at 30°S in the Indian and pacific oceans in 2002–2003 and 2009. Prog. Oceanogr. 146, 89–120. https://doi.org/10.1016/j.pocean.2016.06.005.

Hood, Raleigh R., Ummenhofer, Caroline C., Phillips, Helen E., Janet, Sprintall, 2024. Introduction to the Indian ocean. In: The Indian Ocean and its Role in the Global Climate System. Elsevier, pp. 1–31. https://doi.org/10.1016/B978-0-12-822698-8.00015-9.

Huhn, F., Von Kameke, A., Pérez-Muñuzuri, V., Olascoaga, M.J., Beron-Vera, F.J., 2012. The impact of advective transport by the South Indian ocean countercurrent on the Madagascar plankton bloom. Geophys. Res. Lett. 39 (6), 2012GL051246. https://doi.org/10.1029/2012GL051246. March 28.

Huot, Yannick, Antoine, David, Daudon, Chloe, 2019. Partitioning the Indian ocean based on surface fields of physical and biological properties. Deep Sea Res. Part II Top. Stud. Oceanogr. 166, 75–89. https://doi.org/10.1016/j.dsr2.2019.04.002.

Johnson, Gregory C., Hosoda, Shigeki, Jayne, Steven R., Oke, Peter R., Riser, Stephen C., Roemmich, Dean, Suga, Tohsio, Thierry, Virginie, Wijffels, Susan E., Jianping, Xu, 2022. Argo—two decades: global oceanography, revolutionized. Ann. Rev. Mar. Sci 14 (1), 379–403. https://doi.org/10.1146/annurev-marine-022521-102008. January 3.

Karl, David M., Roger, Lukas, 1996. The Hawaii Ocean Time-series (HOT) program: background, rationale and field implementation. Deep Sea Res. Part II Top. Stud. Oceanogr. 43 (2–3), 129–156. https://doi.org/10.1016/0967-0645(96)00005-7.

Kheireddine, Malika, Mayot, N., Ouhssain, M., Jones, B.H., 2021. Regionalization of the Red Sea based on phytoplankton phenology: a satellite analysis. J. Geophys. Res.: Oceans 126 (10), e2021JC017486. https://doi.org/10.1029/2021JC017486.

Kim, Jihwan, Na, Hanna, 2022. Interannual variability of yellowfin tuna (Thunnus albacares) and bigeye tuna (Thunnus obesus) catches in the southwestern tropical Indian ocean and its relationship to climate variability. Front. Mar. Sci. 9 (April 14), 857405. https://doi.org/10.3389/fmars.2022.857405.

Le Traon, P.Y., 2013. From satellite altimetry to Argo and operational oceanography: three revolutions in oceanography. Ocean Sci. 9 (5), 901–915. https://doi.org/10.5194/os-9-901-2013. October 29.

Lee, Eunsun, Kim, Chanmi, Hanna, Na, 2022. Suppressed upwelling events in the Seychelles–Chagos Thermocline Ridge of the southwestern tropical Indian ocean. Ocean Sci. J. 57 (2), 305–313. https://doi.org/10.1007/s12601-022-00075-x.

Lévy, M., Shankar, D., André, J.-M., Shenoi, S.S.C., Durand, F., De Boyer Montégut, C., 2007. Basin-wide seasonal evolution of the Indian ocean's phytoplankton blooms. J. Geophys. Res.: Oceans 112 (C12). https://doi.org/10.1029/2007JC004090, 2007JC004090.

Longhurst, Alan, 2001. A major seasonal phytoplankton bloom in the Madagascar basin. Deep Sea Res. Oceanogr. Res. Pap. 48 (11), 2413–2422. https://doi.org/10.1016/S0967-0637(01)00024-3.

Marchese, Christian, De La Guardia, Laura Castro, Myers, Paul G., Bélanger, Simon, 2019. Regional differences and inter-annual variability in the timing of surface phytoplankton blooms in the labrador sea. Ecol. Indic. 96, 81–90. https://doi.org/10.1016/j.ecolind.2018.08.053.

Marsac, Francis, Everett, Bernadine, Shahid, Umair, Strutton, Peter G., 2024. Indian ocean primary productivity and fisheries variability. In: The Indian Ocean and its Role in the Global Climate System. Elsevier, pp. 245–264. https://doi.org/10.1016/B978-0-12-822698-8.00019-6.

Marshak, Anthony R., Link, Jason S., 2021. Primary production ultimately limits fisheries economic performance. Sci. Rep. 11 (1), 12154. https://doi.org/10.1038/s41598-021-91599-0.

Martin, Adrian, Boyd, Philip, Buesseler, Ken, Cetinic, Ivona, Claustre, Hervé, Giering, Sari, Henson, Stephanie, et al., 2020. The Oceans' twilight zone must Be studied now, before it is too late. Nature 580 (7801), 26–28. https://doi.org/10.1038/d41586-020-00915-7.

Mayot, Nicolas, D'Ortenzio, Fabrizio, d'Alcalà, Maurizio Ribera, Lavigne, Héloïse, Claustre, Hervé, 2016. Interannual variability of the mediterranean trophic regimes from ocean color satellites. Biogeosciences 13 (6), 1901–1917. https://doi.org/10.5194/bg-13-1901-2016. March 30.

McClain, Charles R., 2009. A decade of satellite ocean color observations. Ann. Rev. Mar. Sci 1 (1), 19–42. https://doi.org/10.1146/annurev.marine.010908.163650.

McPhaden, Michael J., Beal, Lisa M., Udaya Bhaskar, T.V.S., Lee, Tong, Nagura, Motoki, Strutton, Peter G., Yu, Lisan, 2024. The Indian Ocean Observing system (IndOOS). In: The Indian Ocean and its Role in the Global Climate System. Elsevier, pp. 393–419. https://doi.org/10.1016/B978-0-12-822698-8.00002-0.

Menezes, Viviane V., Phillips, Helen E., Schiller, Andreas, Bindoff, Nathaniel L., Domingues, Catia M., Vianna, Marcio L., 2014. South I ndian C ountercurrent and associated fronts. J. Geophys. Res.: Oceans 119 (10), 6763–6791. https://doi.org/10.1002/2014JC010076.

Metzl, Nicolas, Lo Monaco, Claire, Leseurre, Coraline, Ridame, Céline, Fin, Jonathan, Mignon, Claude, Gehlen, Marion, Tuyet Trang Chau, Thi, 2022. The impact of the South-east Madagascar bloom on the oceanic CO_2 sink. Biogeosciences 19 (5), 1451–1468. https://doi.org/10.5194/bg-19-1451-2022. March 10.

Mignot, Alexandre, Claustre, Hervé, Uitz, Julia, Poteau, Antoine, D'Ortenzio, Fabrizio, Xing, Xiaogang, 2014. Understanding the seasonal dynamics of phytoplankton biomass and the deep chlorophyll maximum in oligotrophic environments: a bio-argo float investigation. Glob. Biogeochem. Cycles 28 (8), 856–876. https://doi.org/10.1002/2013GB004781.

Moltmann, Tim, Turton, Jon, Zhang, Huai-Min, Nolan, Glenn, Gouldman, Carl, Griesbauer, Laura, Willis, Zdenka, et al., 2019. A Global Ocean observing system (GOOS), delivered through enhanced collaboration across regions, communities, and new technologies. Front. Mar. Sci. 6 (June 28), 291. https://doi.org/10.3389/fmars.2019.00291.

Moustahfid, Hassan; Marsac, Francis; Gangopadhyay, Avijit, Climate change impacts, vulnerabilities and adaptations: Western Indian Ocean marine fisheries. Impact of Climate Change on Fisheries and Aquaculture: synthesis of current knowledge, adapations, and mitigation options FAO Fisheries and Aquaculture 251–279; Technical Paper No. 627. Rome, FAO.

Munk, Walter, 2000. Oceanography before, and after, the advent of satellites. In: Satellites, Oceanography and Society. Elsevier Oceanography Series. David Hapern, pp. 1–4.

Nagura, Motoki, McPhaden, Michael J., 2018. The shallow overturning circulation in the Indian ocean. J. Phys. Oceanogr. 48 (2), 413–434. https://doi.org/10.1175/JPO-D-17-0127.1.

New, A.L., Stansfield, K., Smythe-Wright, D., Smeed, D.A., Evans, A.J., Alderson, S.G., 2005. Physical and biochemical aspects of the flow across the Mascarene plateau in the Indian ocean. In: Spencer, Tom, Laughton, Anthony S., Flemming, Nic C. (Eds.), Philos. Trans. R. Soc. A Math. Phys. Eng. Sci. 363 (1826), 151–168. https://doi.org/10.1098/rsta.2004.1484.

Owens, W. Brechner, Zilberman, Nathalie, Johnson, Ken S., Claustre, Hervé, Scanderbeg, Megan, Wijffels, Susan, Suga, Toshio, 2022. OneArgo: a new paradigm for observing the Global Ocean. Mar. Technol. Soc. J. 56 (3), 84–90. https://doi.org/10.4031/MTSJ.56.3.8. June 8.

Pauly, D., Christensen, V., 1995. Primary production required to sustain global fisheries. Nature 374 (6519), 255–257. https://doi.org/10.1038/374255a0.

Phillips, Helen E., Menezes, Viviane V., Nagura, Motoki, McPhaden, Michael J., Vinayachandran, P.N., Beal, Lisa M., 2024. Indian Ocean Circulation. In: The Indian Ocean and its Role in the Global Climate System. Elsevier, pp. 169–203. https://doi.org/10.1016/B978-0-12-822698-8.00012-3.

Phillips, Helen E., Tandon, Amit, Furue, Ryo, Hood, Raleigh, Ummenhofer, Caroline C., Benthuysen, Jessica A., Menezes, Viviane, et al., 2021. Progress in understanding of Indian Ocean Circulation, variability, air–sea exchange, and impacts on biogeochemistry. Ocean Sci. 17 (6), 1677–1751. https://doi.org/10.5194/os-17-1677-2021. November 26.

Pond, Stephen, Pickard, George L., 1983. Introductory Dynamical Oceanography, second ed. Butterworth-Heinemann. https://doi.org/10.1016/C2009-0-24288-7.

Prieur, Louis, D'ortenzio, Fabrizio, Vincent, Taillandier, Testor, Pierre, 2020. Physical oceanography of the ligurian sea. In: Migon, Christophe, Nival, Paul, Sciandra, Antoine (Eds.), The Mediterranean Sea in the Era of Global Change 1, first ed. Wiley, pp. 49–78. https://doi.org/10.1002/9781119706960.ch3.

Ras, J., Claustre, H., Uitz, J., 2008. Spatial variability of phytoplankton pigment distributions in the subtropical south pacific ocean: comparison between in situ and predicted data. https://doi.org/10.5194/bg-5-353-2008.

Read, J.F., Lucas, M.I., Holley, S.E., Pollard, R.T., 2000. Phytoplankton, nutrients and hydrography in the frontal zone between the Southwest Indian subtropical gyre and the Southern Ocean. Deep Sea Res. Oceanogr. Res. Pap. 47 (12), 2341–2367. https://doi.org/10.1016/S0967-0637(00)00021-2.

Reid, Joseph L., 2003. On the total geostrophic circulation of the Indian ocean: flow patterns, tracers, and transports. Prog. Oceanogr. 56 (1), 137–186. https://doi.org/10.1016/S0079-6611(02)00141-6.

Rembauville, Mathieu, Briggs, Nathan, Ardyna, Mathieu, Uitz, Julia, Catala, Philippe, Penkerc'h, Cristophe, Poteau, Antoine, Claustre, Hervé, Blain, Stéphane, 2017.

Plankton assemblage estimated with BGC-argo floats in the Southern Ocean: implications for seasonal successions and particle export. J. Geophys. Res.: Oceans 122 (10), 8278–8292. https://doi.org/10.1002/2017JC013067.
Resplandy, L., Vialard, J., Lévy, M., Aumont, O., Dandonneau, Y., 2009. Seasonal and intraseasonal biogeochemical variability in the Thermocline Ridge of the southern tropical Indian ocean. J. Geophys. Res.: Oceans 114 (C7). https://doi.org/10.1029/2008JC005246, 2008JC005246.
Riser, Stephen C., Freeland, Howard J., Roemmich, Dean, Wijffels, Susan, Troisi, Ariel, Belbéoch, Mathieu, Gilbert, Denis, et al., 2016. Fifteen years of ocean observations with the global Argo array. Nat. Clim. Change 6 (2), 145–153. https://doi.org/10.1038/nclimate2872.
Robinson, J., Guillotreau, P., Jiménez-Toribio, R., Lantz, F., Nadzon, L., Dorizo, J., Gerry, C., Marsac, F., 2010. Impacts of climate variability on the tuna economy of Seychelles. Clim. Res. 43 (3), 149–162. https://doi.org/10.3354/cr00890.
Roemmich, Dean, Alford, Matthew H., Claustre, Hervé, Johnson, Kenneth, King, Brian, Moum, James, Oke, Peter, et al., 2019. On the future of Argo: a global, full-depth, multi-disciplinary array. Front. Mar. Sci. 6 (August 2), 439. https://doi.org/10.3389/fmars.2019.00439.
Roemmich, Dean, Johnson, Gregory C., Riser, Stephen, Davis, Russ, Gilson, John, Brechner Owens, W., Garzoli, Silvia L., Schmid, Claudia, Ignaszewski, Mark, 2009. The agro program observing the Global Ocean with profiling floats. Oceanography (Wash. D. C.) 22 (2), 34–43.
Roxy, Mathew Koll, Ritika, Kapoor, Terray, Pascal, Masson, Sébastien, 2014. The curious case of Indian ocean Warming*,+. J. Clim. 27 (22), 8501–8509. https://doi.org/10.1175/JCLI-D-14-00471.1. November 15.
Saji, N.H., Goswami, B.N., Vinayachandran, P.N., Yamagata, T., 1999. A dipole mode in the tropical Indian ocean. Nature 401 (6751), 360–363. https://doi.org/10.1038/43854.
Sarmiento, Jorge L., Kenneth S. Johnson, Lionel A. Arteaga, Seth M. Bushinsky, Heidi M. Cullen, Alison R. Gray, Roberta M. Hotinski, et al. "The Southern Ocean Carbon and Climate Observations and Modeling (SOCCOM) Project: A Review." Prog. Oceanogr. 219 (December 2023): 103130. https://doi.org/10.1016/j.pocean.2023.103130.
Schott, Friedrich A., Dengler, Marcus, Schoenefeldt, Rena, 2002. The shallow overturning circulation of the Indian ocean. Prog. Oceanogr. 53 (1), 57–103. https://doi.org/10.1016/S0079-6611(02)00039-3.
Schott, Friedrich A., Julian, P. McCreary, 2001. The monsoon circulation of the Indian ocean. Prog. Oceanogr. 51 (1), 1–123. https://doi.org/10.1016/S0079-6611(01)00083-0.
Schott, Friedrich A., Xie, Shang-Ping, McCreary, Julian P., 2009. Indian Ocean Circulation and climate variability. Rev. Geophys. 47 (1). https://doi.org/10.1029/2007RG000245, 2007RG000245.
Schwarz, Jill N., 2020. Dynamic partitioning of tropical Indian ocean surface waters using Ocean Colour data — management and modelling applications. J. Environ. Manag. 276, 111308. https://doi.org/10.1016/j.jenvman.2020.111308.
Shutler, Jamie D., Nicolas Gruber, Helen S. Findlay, Peter E. Land, Luke Gregor, Thomas Holding, Richard P. Sims, et al. "The Increasing Importance of Satellite Observations to Assess the Ocean Carbon Sink and Ocean Acidification." Earth Sci. Rev. 250 (March 2024): 104682. https://doi.org/10.1016/j.earscirev.2024.104682.
Sloyan, Bernadette M., Wanninkhof, Rik, Kramp, Martin, Johnson, Gregory C., Talley, Lynne D., Tanhua, Toste, McDonagh, Elaine, et al., 2019. The Global Ocean ship-based hydrographic investigations program (GO-SHIP): a platform for integrated multidisciplinary ocean science. Front. Mar. Sci. 6 (August 7), 445. https://doi.org/10.3389/fmars.2019.00445.
Srokosz, M.A., Quartly, G.D., 2013. The Madagascar bloom: a serendipitous study. J. Geophys. Res.: Oceans 118 (1), 14–25. https://doi.org/10.1029/2012JC008339.
Srokosz, M.A., Robinson, J., McGrain, H., Popova, E.E., Yool, A., 2015. Could the Madagascar bloom Be fertilized by madagascan iron? J. Geophys. Res.: Oceans 120 (8), 5790–5803. https://doi.org/10.1002/2015JC011075.
Stramma, L., Lutjeharms, J.R.E., 1997. The flow field of the subtropical gyre of the South Indian ocean. J. Geophys. Res.: Oceans 102 (C3), 5513–5530. https://doi.org/10.1029/96JC03455.
Taillandier, Vincent, Dimier, Céline, Claustre, Hervé, D'Ortenzio, Fabrizio, Ternon, Jean-Francois, 2024. Oceanographic Data Collection of the Monaco Exploration Indian Ocean Cruise. SEANOE. https://doi.org/10.17882/98833.
Taillandier, Vincent, Wagener, Thibaut, D'Ortenzio, Fabrizio, Mayot, Nicolas, Legoff, Hervé, Ras, Joséphine, Coppola, Laurent, et al., 2018. Hydrography and biogeochemistry dedicated to the mediterranean BGC-argo network during a cruise with RV *tethys 2* in may 2015. Earth Syst. Sci. Data 10 (1), 627–641. https://doi.org/10.5194/essd-10-627-2018.
Talley, L.D., Rosso, I., Kamenkovich, I., Mazloff, M.R., Wang, J., Boss, E., Gray, A.R., et al., 2019. Southern Ocean biogeochemical float deployment strategy, with example from the greenwich meridian line (GO-SHIP A12). J. Geophys. Res.: Oceans 124 (1), 403–431. https://doi.org/10.1029/2018JC014059.
Talley, Lynne D., Baringer, Molly O., 1997. Preliminary results from WOCE hydrographic sections at 80°E and 32°S in the central Indian ocean. Geophys. Res. Lett. 24 (22), 2789–2792. https://doi.org/10.1029/97GL02657. November 15.
Talley, Lynne D., Johnson, Gregory C., Purkey, Sarah, Feely, Richard A., Wanninkhof, Rik, 2017. Global Ocean Ship-Based Hydrographic Investigations Program (GO-SHIP) Provides Key Climate-Relevant Deep Ocean Observations.
Talley, Lynne D., Pickard, George L., Emery, William J., Swift, James H., 2011. Indian ocean. In: Descriptive Physical Oceanography. Elsevier, pp. 363–399. https://doi.org/10.1016/B978-0-7506-4552-2.10011-3.
Tanhua, Toste, McCurdy, Andrea, Fischer, Albert, Appeltans, Ward, Bax, Nicholas, Kim, Currie, DeYoung, Brad, et al., 2019. What we have learned from the framework for Ocean Observing: evolution of the global Ocean Observing system. Front. Mar. Sci. 6 (August 20), 471. https://doi.org/10.3389/fmars.2019.00471.
Taylor, Sarah F.W., Roberts, Michael J., Milligan, Ben, Ncwadi, Ronney, 2019. Measurement and implications of marine food security in the western Indian ocean: an impending crisis? Food Secur. 11 (6), 1395–1415. https://doi.org/10.1007/s12571-019-00971-6.
Thompson, B.J., Crease, J., Gould, John, 2001. Chapter 1.3 the origins, development and conduct of WOCE. Int. Geophys. 77, 31–VIII. https://doi.org/10.1016/S0074-6142(01)80110-8. Elsevier.
Tripathy, Sarat C., Sabu, P., Patra, Sivaji, Naik, Ravidas K., Sarkar, Amit, Venkataramana, Vankara, Kerkar, Anvita U., Pandi, Sudarsanarao, 2020. Biophysical control on variability in phytoplankton production and composition in the South-western tropical Indian Ocean during monsoon 2014. Front. Mar. Sci. 7 (July 16), 515. https://doi.org/10.3389/fmars.2020.00515.
Uz, B. Mete, 2007. What causes the sporadic phytoplankton bloom southeast of Madagascar? J. Geophys. Res.: Oceans 112 (C9), 2006JC003685. https://doi.org/10.1029/2006JC003685.
Vianello, Patrick, Ternon, Jean-François, Demarcq, Hervé, Herbette, Steven, Roberts, Michael J., 2020. Ocean currents and gradients of surface layer properties in the vicinity of the Madagascar ridge (including seamounts) in the south west Indian Ocean. Deep Sea Res. Part II Top. Stud. Oceanogr. 176, 104816. https://doi.org/10.1016/j.dsr2.2020.104816.
Vidya, P.J., Ravichandran, M., Murtugudde, R., Subeesh, M.P., Chatterjee, Sourav, Neetu, S., Nuncio, M., 2020. Increased cyclone destruction potential in the southern Indian ocean. Environ. Res. Lett. 16 (1), 014027. https://doi.org/10.1088/1748-9326/abceed.
Vinayachandran, Puthenveettil Narayana Menon, Masumoto, Yukio, Roberts, Michael J., Huggett, Jenny A., Halo, Issufo, Chatterjee, Abhisek, Amol, Prakash, et al., 2021. Reviews and syntheses: physical and biogeochemical processes associated with upwelling in the Indian ocean. Biogeosciences 18 (22), 5967–6029. https://doi.org/10.5194/bg-18-5967-2021. November 23.
Wong, Annie P.S., Wijffels, Susan E., Riser, Stephen C., Pouliquen, Sylvie, Hosoda, Shigeki, Roemmich, Dean, Gilson, John, et al., 2020. Argo data 1999–2019: two million temperature-salinity profiles and subsurface velocity observations from a global array of profiling floats. Front. Mar. Sci. 7 (September 15), 700. https://doi.org/10.3389/fmars.2020.00700.
Yamagami, Y., Tozuka, T., 2015. Interannual variability of South Equatorial current bifurcation and western boundary currents along the Madagascar coast. J. Geophys. Res.: Oceans 120 (12), 8551–8570. https://doi.org/10.1002/2015JC011069.
Yamagata, Toshio, Behera, Swadhin, Doi, Takeshi, Luo, Jing-Jia, Morioka, Yushi, Tozuka, Tomoki, 2024. Climate phenomena of the Indian ocean. In: The Indian Ocean and its Role in the Global Climate System. Elsevier, pp. 103–119. https://doi.org/10.1016/B978-0-12-822698-8.00009-3.
Yokoi, Takaaki, Tozuka, Tomoki, Yamagata, Toshio, 2008. Seasonal variation of the Seychelles dome. J. Clim. 21 (15), 3740–3754. https://doi.org/10.1175/2008JCLI1957.1. August 1.